University of Stavanger

Faculty of Science and Technology

MASTER'S THESIS

Study program/ Specialization: Petroleum Engineering / Well Engineering	Spring semester, 2018 Open
Writer: Diego Felipe Acevedo Parra	…… (Writer's signature)
Faculty supervisor: Rune W. Time Milad Khatibi	
Thesis title: Experimental Study of Particle Dynamics in Circular Channel Flow	
Credits (ECTS): 30	
Key words: Particle transport Secondary flow Rolling, sliding and saltating motion PIV Bed geometry	Pages: 83 + supplemental material/other: USB Stavanger, 15th June 2018

Title page for master's thesis
Faculty of Science and Technology

Experimental Study of Particle Dynamics in Circular Channel Flow

Master's thesis spring 2018

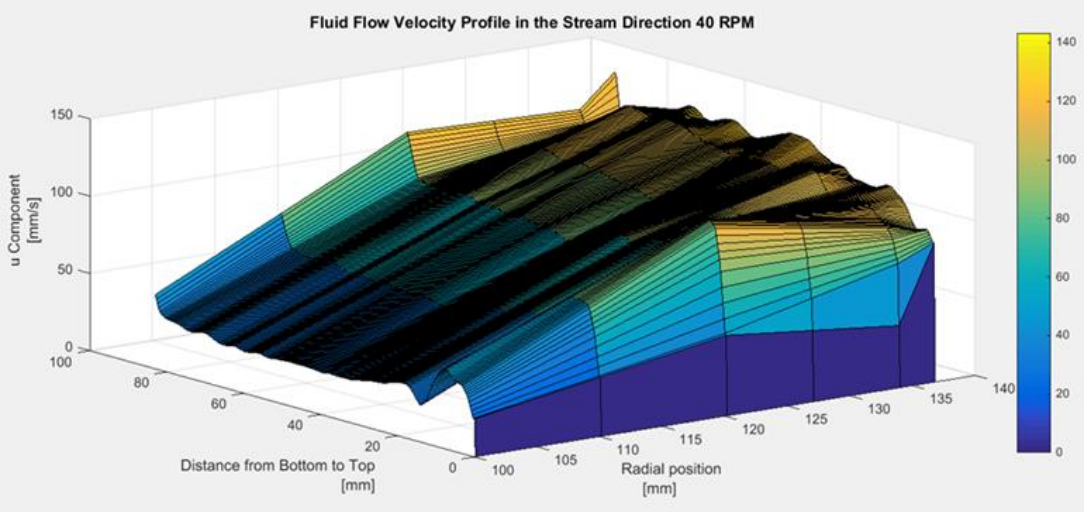

Diego Felipe Acevedo Parra

Department of Petroleum Engineering

Faculty of Science and Technology

University of Stavanger

15.06.2018

Abstract

The study of liquid-particle interaction is the vital importance in many industries, especially for the petroleum well drilling and hole-cleaning operations. The data obtained from laboratory-scale experiments, simulations, and analytical models is a key factor for the success of highly costly operations in the oil & gas industry; such as drilling of oil and gas wells (cuttings transportation), gravel packing, transport of coarse material, and proppant during hydraulic fracturing.

This experimental work aims to study the liquid-particles flow in a continuous annulus channel (cylindrical cell). The setup was made of two coaxial cylinders that were fixed to the bottom plate of an "aquarium" box. The upper plate on top of the cylinders could rotate and shear the liquid inside the channel. The liquid flow, in turn, dragged the particles that were added to the test fluid beforehand. The experiments were pretended to be carried out for three different particle sizes (0.5, 1.0 and 2.0 mm), different concentrations (thin layer = one to two particle size, and thick layer = more than 3 times particle size) as well as different rotation speed (RPM) and initial bed-forms (plane and single dune).

The initial step was to perform a Particle Image Velocity (PIV) analysis to measure the liquid velocity profile in 3D: angular, radial and axial velocities. An azimuthal and close to plane Couette flow was expected, however, the results obtained from the PIV showed a rapid increase of the liquid velocity near the bottom wall, due to the action of a secondary flow inside the channel. The secondary flow went inwards at the bottom of the channel and outwards at the top.

Once the PIV technique was done, spherical aluminum particles were added into the channel and the particle flow involved during the experiments were recorded by two high-speed cameras (recording images from bottom view and frontal view). In this case, parameters such as bed morphology, particles movements and velocity, as well as bed height and the geometry of the deposit among others were analyzed. It is important to notice that due to the presence of centrifugal force the generated secondary flow drags the particles inwards to the inner wall at the channel bottom differentiating the actual experiment from the well-known flume experiments. The current annular channel can be seen as a simplified version of the annulus formed between the drill pipe and casing with the drill string rotating (upper plate rotation).

Table of Contents

Preface

This master's thesis represents the end of a dream; my master in Petroleum Engineering. It was two years of constant hard work and sacrifices to make this dream a reality. I am very proud of what I have accomplished through this period where I always tried to do the best in order to achieve the best possible results, including this thesis work.

First and foremost, I want to thank God for all the blessings and because he never forsakes me.

I would like to offer my special thanks to Professor Rune time, my main supervisor, for his unique and graphic explanations, excellent comments and constructive recommendations during the planning and development of this thesis work.

I would like to express my deep gratitude to Milad Khatibi, my co-supervisor, for his great support, patience and guidance during the development of this experimental project. His willingness to answer my questions at any time has been very much appreciated.

My special thanks are extended to my friends, for the long discussions about technical and nontechnical topics and wonderful extra academic moments. Especially to Milton Angulo (my classmate/flatmate) how became my brother.

Finally, I wish to thank my lovely family for their unconditional love and support. Seeing you smile and being proud of my achievements is my main motivation and greatest reward.

Nomenclature

Symbol	Definition
A_F	Exposed particle area to the flow or projected area
C_D	Drag coefficient
C_L	Lift coefficient
h_f	Fluid column
Re_c	Channel Reynolds number
Re	Reynolds number
ρ	Density
ρ_p	Particle density
τ_r	Radial shear stress
τ_a	Azimuthal shear stress
τ_{bc}	Critical bed shear stress
d	Particle diameter
g	Gravity
F_D	Drag force
F_F	Fluid force
F_G	Gravity force
F_L	Lift force
T_v	Response time
T_c	Average time between particle-particle collision

u	Speed of the particle relative to the fluid
U_{Lid}	Lid rotation speed
U_w	Lid angular velocity at mean radius
U_F	Local fluid/liquid velocity
W	Angular velocity
R	Mean radius
μ_F	Fluid viscosity
α_p	Particle concentration

Greek symbols

Symbol	Definition
τ	Shear stress
γ	Shear rate
θ	Shields number
$\emptyset$	Mean diameter
ρ	Density
μ	Dynamic viscosity
α	Concentration
Δt	Time difference
ΔS	Distance difference

Subscripts

Symbol	Definition
D	Drag
f	Fluid
P	Particle
b	Bed
r	Radial
a	Azimuthal

Abbreviations

Symbol	Definition
PIV	Particle image velocimetry
PTV	Particle tracking velocimetry
FPS	Frames per second
RPM	Revolutions per minute
OD	Outer diameter
ID	Inner diameter

List of Figures

List of Tables

Chapter 1

1) Introduction

Liquid-particle interaction is of vital importance in many industries, especially for the oil business. The information collected from experimental studies related to particle dynamics is a key factor to study, understand and improve operations in the petroleum industry such as wellbore cleaning (cutting transport), gravel packing, hydraulic fracturing (propane pumping and displacement), erosion of sand during oil production, among others.

It is important to define the term particle since it is a general word that depending on the area of studies it is used to refer to different concepts, for instance, nuclear physicists and geologists may employ this word in a different way (Clift, Grace, & Weber, 2005). Then, following the concept of (Clift et al.), for this thesis; a particle is as a self-contained and non-deformable solid body with a recognizable interface with liquid or gas surrounding it.

Great interest in bed-load particles transportation were developed in the 1940's and 50's when scientists started to focus more on this topic; (Meyer-Peter & Müller, 1948) empirical bed-load transport formula, (Einstein, 1950) and (Bagnold, 1954) carried out a bed-load transport equation based on theory; conjecturing the main mode of bedload transportation as a saltation. More recent (Fernandez Luque & Van Beek, 1976) measured the mean rate of the bed load transport, particle velocity, saltation lengths and number of particles deposited per unit are for water flow, and (Charru, Mouilleron, & Eiff, 2004) reports longitudinal particle velocity, length and duration of the particle flights and surface density of moving particles for a viscous flow . During these time these and other authors have tried to solve and get unique concepts/models, however as it was pointed out by (Fernandez Luque, 1974) the mechanic of bed load transport were not yet completely understood and it remains the same nowadays. This is clearly understandable due to the high complexity of the situation; the difficulty of controlling and determining the flow and particle parameters, such as turbulent flow near the bed, size, shape, and roughness of the particles (Charru et al., 2004).

One of the fields where more attention has been given is the transport of sediments, however this still escapes from a clear understanding and efficient predictive laws (Charru, Bouteloup, Bonometti, & Lacaze, 2016). Equations and models still used remain based on correlations and semi-empirical equations that are derivate based on specific conditions, observations and experimental data. "Most of the laws for bed load transport proposed in the literature consist of semi-empirical equations derived from a fit of data acquired in flume experiment"(Lajeunesse, Malverti, & Charru, 2010). The same situation is found in the oil industry were the calculations of the parameters of particle transport and bed motion have been developed based on assumptions/local conditions. For example, during open hole gravel packing even though that the slurry is in contact with the formation face, zero roughness is

assumed omitting an extra pressure drop. These kinds of assumptions are totally necessary to decrease the grade of complexity of the problems but they also diminish the final operation outcome.

When working with particle motion by streamflow one of the principal parameter is the well-known Shields number (1936) which is the ratio between the fluid force on particles and the weight of the particles. This parameter represents the threshold of the incipient motion of the particles, in other words, the necessary minimum shear stress to move a particle. Then as the streamflow velocity increases, at a certain point, the topmost particles on the bed are entrained into the liquid. This happens at the moment when the fluid forces exceed the stabilizing force due to the submerged weight (Dey & Ali, 2017).

Once the threshold of incipient motion is achieved, particles will move in different patterns forming the bed load or moving layer; the particles of the load which travel in direct contact or very close to the bed. (Francis, 1973) studied the motion of single particles over a fixed bed of a water stream in the laboratory, observing three main modes of movements:

Rolling: This type of movement is compared to the motion of the wheels of a car along the road surface, in other words, particles role in contact with the bed.

Saltation: Particle describes a ballistic motion close to the bed so it is not very much affected by turbulence. This mode of movement does not have a unique definition since it may vary for different researchers. For example, according with (Francis) particles rise up about 2 to 4 particle diameter about the bed and then it returns and in (Bagnold, 1973) Williams's experiments there was a saltation zone with a well-defined celling of 8 particle diameter . The main point about this is how to determine or define the maximum height that the saltating particle can achieve without entering in the turbulence and being transported in suspension for certain time.

Suspension: particles move in "leaps" for longer distances before falling back. This mode of transportation is distinct from saltation by the length and the trajectory of the particles, in this case sinuous trajectories are observed. In other words, particles are lifted away from the bed to a region where they are affected by turbulence (John Southard, Fall 2006).

As it was mentioned, once the threshold of movement is overcome the particles start entraining into the liquid as a rolling or sliding motion. With further increase in the flow intensity, the particles rise up, performing short jumps along the bed without being affected by turbulence, known as saltating or lifting mode of transport (Dey & Ali, 2017). And with a further increase in the flow velocity the particles will be transported in suspension. In a broader picture; at very slow flow speeds the bed maintains a plane surface, then increasing the speed a new bed form appears; ripples. These ripples are then replaced by dunes which are distinguished by large amplitude and wavelength. If the flow is increased further a plane bed is generated again by the flattening of the dunes (Cocks, 2005) .

The majority of experiments carried out at laboratories to study the dynamic of a bed of particles have been performed by means of flumes which are defined by (John Southard, Fall 2006) as "laboratory channel through which liquid is passed in order to study hydraulic processes and phenomena under controlled conditions." Some of the advantages of this type of setups are their simple and well-known construction, the ease of establishing the initial bed and relatively easy observation and measurement of the main parameters involved during the process. On the other hand, one of the main weaknesses is that the system must be fed with both particles and liquid requiring a complex extra system to ensure constant and exact supply, mass conservation when necessary. This might disrupt the bed form (ripple) dynamic (Betat, Frette, & Rehberg, 1999).

For this thesis work, we do not have a flume as a laboratory channel. In this case, the experimental setup used is a rotational cell where liquid with particles are placed in the channel formed by two fixed concentric cylinder walls and an upper plate (lid) which rotates, shearing the liquid. Now, for the rotational cell, we have the action of the centripetal/centrifugal force that creates a toroidal flow dragging the particles to inwards and outwards at the bed surface and at near the lid respectively. As far as the author knows there are very few reported cases where similar laboratory set-up has been utilized; (Betat et al., 1999; Charru et al., 2004). In the latter, a series of experimental measures were carried out for a unique particle diameter in silicon oil; parameters such as particle velocity, bed thickness, length and duration of the particle flights and surface density of moving particles were observed by means of a CCD camera and an ultrasonic probe. For the experiments, the particles Reynolds number and the channel Reynolds number were limited to maximum upper bounds in such a way that the effect of the secondary flow was negligible. (Charru et al.) also developed a deposition and erosion model for a bed sheared by a viscous flow.

(Lajeunesse et al., 2010) presents a summary of some of the equations used to describe the moving layer rate that have been derived from a fit of experimental data and-or theoretical derivation for a turbulent flow with the bed load rate in function of the shear stress at bed and the critical shear stress (incipient motion of the particle). Moreover, the saltation lengths, the average particle velocity, the height of the bed, among others are also summarized. The main point here is that the majority of these correlations were derived based on data from empirical experiments in flumes either closed or open where no secondary flow is present through a lot of time. As a result, it is not the aim of this thesis to develop new correlations that includes the effect of the secondary flow, this kind of work requires much more time and more in-depth specialization.

(Franklin & Charru, 2009) experimentally studied what happens with a pile of beads placed in the in a rectangular closed conduit when these particles are sheared by water. They found that the water rapidly deformed the initial accumulation of piles and a bed form like barchan dune is originated. This "solitary like" dune moves downward maintaining its shape (particles were not fed). Furthermore, the

velocity and morphology of the isolated dune were observed. In the present experiment, the same situation will be studied with the aim to observe the effect of the secondary flow over the morphology and velocity of the resulting bed form.

The aim of this work is to study the particle bed motion, particle bed morphology among other features in a circular channel by means of experimental observations.

First, determine the velocity profile in the annular channel for water at different velocities of the upper plate (rpm) from the outer to the inner wall in the stream direction (azimuthal direction), employing Particle Image Velocimetry (PIV).

Determine threshold of motion for the biggest particle size used in the actual experiments; starting at 20 RPM with an increase of 20 RPM. This in order to know the minimum RPM needed and define which lid rotation speed is going to be used in the experiments. It is important to notice that this is not a detailed study of the particle incipient motion since this will imply a very low increase of the angular velocity.

Identify the mode of particle transportation for 2 types of particles size at two different angular velocities; recording the experiment with high-speed cameras and by visual tracking of the particles.

Measure the instantaneous velocity and show the path-line of the moving particles for three cases; single size particle of mean diameter d=2 mm, a mixture of particles of d=1 mm & d=2 mm, and single size particle of d=1 mm. This will be done for the upper's plate spindle speed of 120RPM, from the initial state (time zero) to the steady state of the system.

Study the effect of increasing the particle concentration for single size particles and a mixture of particles with respect to the bed geometry.

Understand some features of the dynamics of isolated dunes in a cylindrical cell, notably if the particles could be transported as single dune under a given constant lid rotation speed.

In short, the main objective is to understand some features of the particle dynamics in a cylindrical cell when the secondary flow is present for different particle size, upper plate rotation (rpm), particle concentration, and to determine the fluid flow profile by means of PIV. To the author's knowledge, this situation has not been yet studied.

Chapter 2

2) Theory

2.1) Fluid Rheology

Fluids are classified as Newtonian or non-Newtonian based on the viscosity behaviour as a function of principally the shear stress and the shear rate.

2.1.1) Newtonian Fluids

Newtonian fluids are named after Sir Isaac Newton who described the flow behaviour of fluids with a simple linear relation between shear stress, τ and shear rate γ (Rheosense). This linear relation is given by:

$$\tau = \frac{F}{A} = \mu\gamma$$

where the proportionally constant μ is the viscosity of the fluid. In other words, a Newtonian fluid is a fluid in which its viscosity remains constant independently of the rate of shear at a constant temperature. Some of the well-known examples of Newtonian fluids are water and honey (Rheosense). In this thesis, water is used for all the experiments.

2.1.2) Non-Newtonian Fluids

In contrast to Newtonian Fluids, non-Newtonian fluids either do not display a linear relationship between shear stress and shear rate (shear thinning or thickening), have a yield stress, or viscosity that is dependent on time or deformation history (Thixotropic fluids) (Rheosense). In other words, the viscosity of non-Newtonian fluids changes with the amount of shear applied that is the same as the viscosity is dependent on the shear stress. Practically speaking most fluids are non-Newtonian and some examples are the drilling fluids, toothpaste, and ketchup.

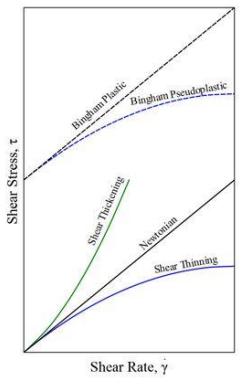

Figure 1: Shear stress as function of shear rate for several kinds of fluids (Rheosense)

2.2) Secondary flow

In a three-dimensional pipe and channel flow, the flow is comprised of two components; the primary flow and the secondary flow. The primary flow is parallel to the main direction of fluid motion and the secondary flow is perpendicular to this. The most known situation where secondary flows occur is when a fluid flows around a bend in a pipe. Besides the previous situation, another typical case where secondary flows take place is in spinning fluids, for example, in a stirred cup. There is a balance between the centrifugal force and the radial pressure gradient. However, near a boundary, drag on the fluid leads to a lower velocity and the centrifugal force can no longer balance the pressure gradient. This results in a secondary flow of the fluid in the radial direction, ("Secondary flow," 2011). In The figure below the secondary flow that arises in the set up here utilized is shown.

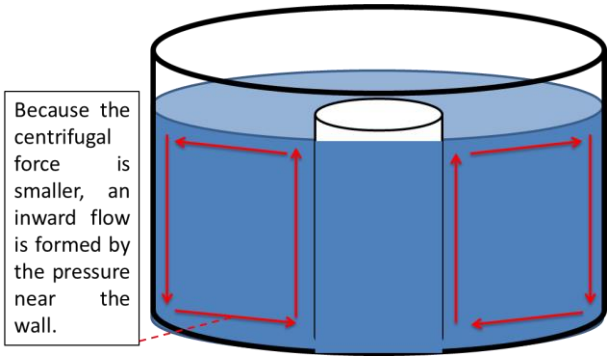

Figure 2: Sketch of secondary flow in the experimental set-up.

As it is displayed in Figure 2, the secondary flow is directed outwards in the upper half of the fluid layer (close to the uppers plate or lid) and inwards in the lower half (close to the bottom of the set up). (Charru et al., 2004) presents the ratio of the radial to the main azimuthal shear stress which is obtained by balancing the radial pressure gradient due to centrifugal forces with the viscous resistance:

$$\delta P_{radial} = \frac{\rho_f U_w^2}{R}; \qquad Viscous\ resistance = \frac{\mu W_f}{h_f^2}$$

Where

R : Mean radius; distance until the midpoint of the annular channel .
W_f : Radial velocity
U_w : Lid angular velocity at mean radius
h_f : Water column

Then, from the previous two equations the ratio of the radial velocity to the angular velocity

$$\frac{W_f}{U_w} = \frac{\rho_f h_f^2 U_w}{\mu R}$$

By definition the channel Reynolds number

$$\mathrm{Re}_c = \frac{\rho_f h_f U_w}{\mu}$$

Then, the ratio of the radial velocity to the angular velocity can be written as

$$\frac{W_f}{U_w} = \frac{\mathrm{Re}_c h_f}{R}$$

Finally from the above equations, the ratio of the radial to main azimuthal shear stress can be written as (Charru et al., 2004):

$$\frac{\tau_r}{\tau_a} = c \ \mathrm{Re}_c \frac{h_f}{R}$$

where c is a constant depending on the aspect ratio of the channel but it is not clearly stated how to calculate this parameter. In the case where the channel Reynolds velocity is low the radial bottom shear stress is small compared with the azimuthal component and as a results, the secondary flow due to the centrifugal effects can be negligible.

2.3) Properties of dispersed phase flows

2.3.1) Response time

The time require for a particle to respond to a change in flow velocity is called the momentum response time. This parameter is important in establishing non-dimensional parameters to characterize the flow (Schwarzkopf, Sommerfeld, Crowe, & Tsuji, 2011). For a low Reynolds number, in the Stokes flow region, the momentum response time is

$$T_V = \frac{\rho_p d^2}{18\mu_f}$$

Where μ_f is the viscosity of the continuous phase, ρ_p is the density of the particle, and d is the diameter of the particle.

2.3.2) Dilute vs. dense flows

A flow where the particle motion is controlled by the fluid forces (drag and lift) is classified as a dilute dispersed flow. While a flow in which the particle motion is controlled by collisions or continuous contact among particles is called a dense flow. In order to have an idea of the nature of the

flow, whether the flow is dilute or dense, the ratio of the momentum response time of a particle to the time between collisions is used. The flow is considered dilute if

$$\frac{T_V}{T_C} < 1$$

"Where Tc is the average time between particle-particle collisions because the particles have enough time to respond to the local fluid dynamic forces before the next collision" (Schwarzkopf et al., 2011) . On the contrary, the flow is dense if

$$\frac{T_V}{T_C} > 1$$

This means that the particle has no time to respond to the fluid dynamic forces before the next collision.

As it can be anticipated there are many mechanisms that are responsible for the particle-particle collisions so it is difficult to set the limits of dilute and dense flows. However, as it is shown in the figure 3 the magnitude of the particle volume fraction, α_p can provide a general indicator (Schwarzkopf et al., 2011).

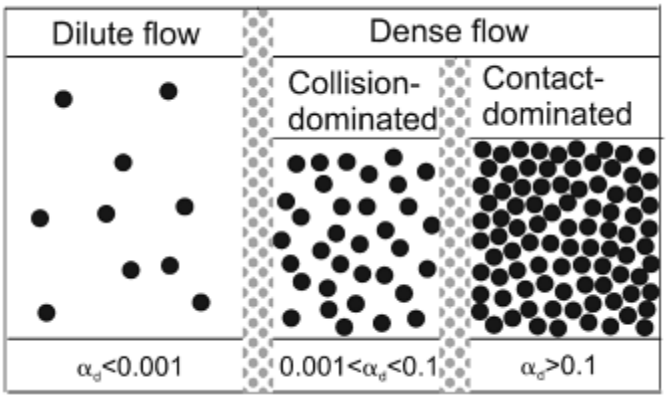

Figure 3: Flow regimes for dilute and dense flows (Schwarzkopf et al., 2011)

The dense flow regime is divided into collision-dominated and contact-dominated regimes. In the collision-dominated flow regime ($0.001 < \alpha_p < 0.1$) particles collide and rebound with a different trajectory. The time during contact is small compared with the time between collisions. For the contact-dominated regime ($\alpha_p > 0.1$) particles are in continuous contact and the contact forces are responsible for particle motion. Lastly, the flow can be considered as dilute for particle volume fraction < 0.001, (Schwarzkopf et al., 2011).

2.4) Particle interactions

2.4.1) Drag

The drag force is the force created by the flow of a fluid around a body that tends to sweep the object along the direction of the flow. Two different kinds of drags; skin friction drag and form drag can take place. The first one occurs on surfaces of objects that are long in direction of flow compared to their height (for example, flow in a pipe) and the second one in objects that are tall in comparison to the length (for example, the pier of a bridge). These two different types of drag no always occur separately, on the contrary, a body usually experiences both skin friction drag and form drag and in this case, the sum of both gives the total drag. It is no easy to predict the drag force by means of purely theoretical methods, so the drag coefficient (C_D) concept based on experimental data is commonly used (*Fluid Mechanics D203*).

$$C_D = \frac{Resistance\ force}{Dynamic\ pressure * projected\ Area} = \frac{2 * F_d}{\rho_f * u^2 * A_f}$$

Where

F_d : drag force
ρ_f : mass density of the fluid
A_f : exposed particle area to the flow or projected area
u : is the flow speed of the object relative to the fluid

In general, the drag coefficient will depend on the particles shape and orientation with respect to the flow as well as the flow parameters such as Mach number, Reynolds number, turbulence level, etc. Schwarzkopf et al. (2011).

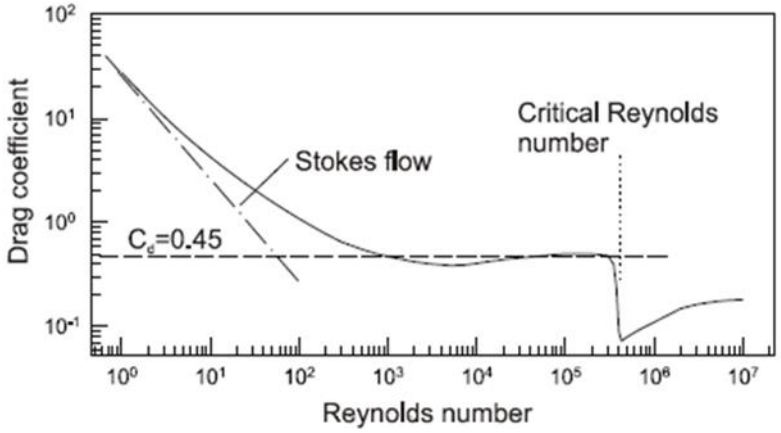

Figure 4: Variation of the drag coefficient of a sphere with Reynolds number(Schwarzkopf et al., 2011).

The figure above shows the variation of the drag coefficient with Reynolds number (Re) for a non-rotating sphere. At very low Reynolds numbers (Re<0.2) the drag coefficient varies inversely with Reynolds number. This is known as the Stokes flow regime where the flow keeps attached to the sphere all the way around. With increasing Re the drag coefficient approaches a nearly constant value which is referred to as the inertial range. For 750 < Re < $3.5x10^5$ the drag coefficient varies by only 13% form C_D=0.445. With increasing Reynolds number there is a sudden decrease in the drag coefficient at the critical Reynolds number, Schwarzkopf et al. (2011).

For Re<0.2 the drag coefficient is expressed as:

$$C_D = \frac{24}{Re}$$

For 0.2 < Re < 500 the flow is called Allen flow and the drag coefficient can be calculated by

$$C_D = 18.5 * Re^{-0.6}$$

For 500 < Re < 10^5, the drag coefficient is approximately constant C_D = 0.44.

On the other hand, a correlation that covers the range 0.2 < Re <10^5 is

$$C_D = \frac{24}{Re} + \frac{6}{1+\sqrt{Re}} + 0.4$$

Finally the drag force can be expressed as follows:

$$F_D = \frac{1}{2} C_D \, \rho_f \, u^2 A_f$$

There are many mechanisms responsible for the relative velocity between particles such as local turbulence, carrier-flow velocity changes, particle-wall impact and so on.

2.4.2) Particle lift forces

Lift forces on a particle are due to particle rotation. This rotation may be generated by a velocity gradient or may be imposed from other sources such as particle contact and rebound from a surface (Schwarzkopf et al., 2011).

Saffman lift force

Figure 5 shows the pressure distribution on a particle as a result of the velocity gradient. On the top of the particle, the velocity is higher than at the bottom which gives origin a low and a high pressure at the top and bottom respectively; so this pressure difference gives rise to a lift force.

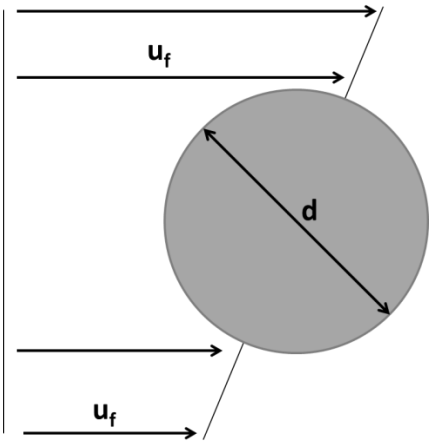

Figure 5: Particle in a shear flow (Schwarzkopf et al., 2011)

2.4.3) Body forces

The product of the particle mass and the gravity (acceleration) gives rise to the most common body force, for a particle submerged in a fluid; this is called the submerged weight. Besides this force, there are others body forces, such as the Coulomb forces and the Thermophoretic forces which may be important depending on the situation.

2.5) Particle-Particle Interaction

Particle-particle collision has a significant effect in dense particle flows. As the number of particles increases, particles collide with each other and the loss of particle kinetic energy due to inter-particle collision cannot be ignored. With respect to particle-particle interactions in multiphase flow dynamics, two phenomena are identified; collision and contact. These two phenomena do not differ significantly from the viewpoint of physics however the modeling approach is different for each. In this case, collision is defined as merely contact with short time duration. For collision and contact, two models are normally used, the hard sphere model and the soft sphere motel,(Schwarzkopf et al., 2011).

The hard sphere model is based on the impulsive force, which is defined by the integral of the force acting on a particle versus time. With the hard sphere model, the post-collisional velocities and rotation are determined as a function of the pre-collisional conditions, coefficient of restitution and coefficient of friction (Johnsen, 2014). This model is only applicable to binary collisions (Schwarzkopf et al., 2011).

The soft sphere model describes the particle history during the collision process and is modeled by using mechanical elements such as spring and a dash-pot. The model is also known as Discrete Element Method (DEM) or Distinct Element Method, (Johnsen, 2014). The applicability of this model is wider than the hard sphere model but it requires longer computation time.

2.5.1) Van der Waals force

Inter-particle forces due to particle wetness, electrostatic charges, and van der Waals forces are known to cause adhesion of a particle to a wall or onto another particle (Schwarzkopf et al., 2011). This kind of force was observed at the beginning of the experiments; see figure below. Here particles agglomerate in the annular channel forming globes. This phenomenon arises when the particles encapsulate small air bubbles (particles wetting) so in order to avoid the agglomerations particles were washed with Ethanol before they were placed in the annular channel. This reduces the surface tension and the particles can move freely.

Figure 6: Particles agglomeration in the annular channel

2.5.2) Particle-wall interaction

When studying fluid-particle flows contained within walls such as pipe flows, channel flows and fluidized beds one encounters the problem of particle-wall interaction. This interaction comprises two categories: hydrodynamic interaction due to the proximity of a wall and mechanical interaction caused by contact with the wall. The Saffman lift force is an example of the hydrodynamic interaction due to the velocity gradient near the wall, (Schwarzkopf et al., 2011).

The treatment of the mechanical behavior associated with particle-wall interaction depends on the inertia of the particle. When a massive particle crashes with a wall, it rebounds but loses kinetic energy due to friction and inelastic effects. For a very small particle approaching a wall, molecular forces become dominant compared with the inertial force. As a result, the particle is captured by the wall due to cohesive forces, and neither rebounds from nor slides along the wall. This cohesive force is identified as the van de Waals force (Schwarzkopf et al., 2011).

2.6) Particle transport

2.6.1) Incipient motion or threshold of movement

When working with particle motion by streamflow one of the principal parameter is the well-known Shields number (1936), θ, which is the ratio between the fluid force on particles and the weight of the particles. This parameter represents the threshold of the incipient motion of the particles, in

other words, the necessary minimum shear stress to move a particle. Then as the streamflow velocity increases, at a certain point, the topmost particles on the bed are entrained into the liquid.

$$\theta = \frac{\tau_{bc}}{(\rho_p - \rho_f) * g * d} = \frac{\mu\gamma}{(\rho_p - \rho_f) * g * d}$$

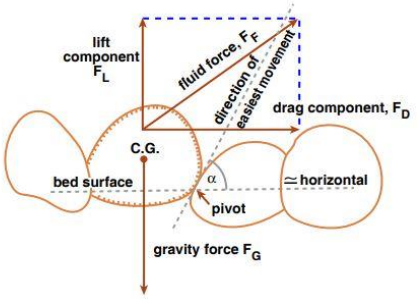

Figure by MIT OpenCourseWare.

Figure 7: Lift and drag on a bed particle, (John Southard, Fall 2006)

After the first particle is moved, more particles are going to be entrained or transported by the effect of the flow. In general, the possible modes of particle transport or modes of entrainment are rolling, sliding and lifting. The particle or sediment transport in rolling, sliding and saltating or lifting modes is known as bedload transport.

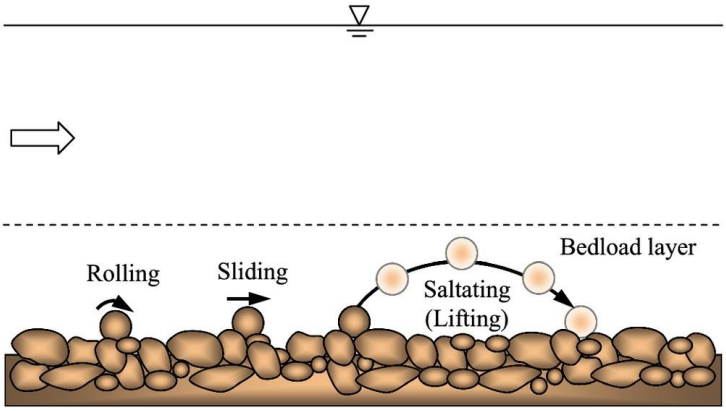

Figure 8: Schematic of bedload transport, (Dey & Ali, 2017)

2.6.2) Sliding mode

In this mode, the instantaneous drag force overcomes the frictional resistance at the points of contact of the particle and the bed particles, (Dey & Ali, 2017), see Figure 9-a).

2.6.3) Rolling mode

It is important to notice although the rolling mode for a spherical particle is the most plausible mode of entrainment, the sliding mode can be also feasible. In this case, when the particle is on the

verge of rolling, the moment balance of the force system about the pivoting point fulfills the criterion: $M_o \geq M_s$ (Dey & Ali, 2017), see Figure 9-b).

2.6.4) Saltating mode

In this mode, the instantaneous lift force exceeds the submerged weight of the solitary particle where the vertical force balance thus yields to the criterion: $F_L \geq F_G$. The lift force is originated from the pressure between the bottom and the top of the particle due to a sharp velocity gradient near the bed, (Dey & Ali, 2017), see Figure 9-c).

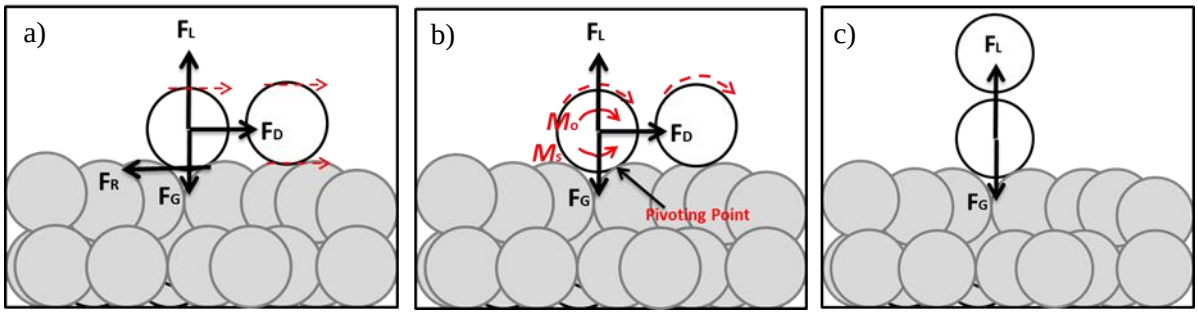

Figure 9: Schematic of different modes of entrainment: a) sliding mode, b) rolling mode, c) lifting mode. Modified from (Dey & Ali, 2017)

The instantaneous drag force (F_D), the submerged weight (F_G), and the instantaneous lift force are (F_L):

$$F_D = \frac{1}{2} C_D \rho_f u^2 A_f$$

$$F_G = \frac{\pi}{6} d^3 (\rho_p - \rho_f) g$$

$$F_L = \frac{1}{2} C_L \rho_f u^2 A_f$$

Where C_L = lift coefficient. This coefficient varies widely, (Dey & Ali, 2017) assumed an average value of C_L =0.2.

Chapter 3

3) Methodology

3.1) Experimental setup

Experiments are performed in an annular channel created by two coaxial cylinders that are fixed to the bottom plate of an aquarium; both the aquarium and the cylinders are made of transparent acrylic. The width and the height of the channel created by the two cylinders are 44 mm and 85 mm respectively [see Figure 10]. The lid or upper plate is designed to be easily removable such as for filling of the channel with liquid and particles.

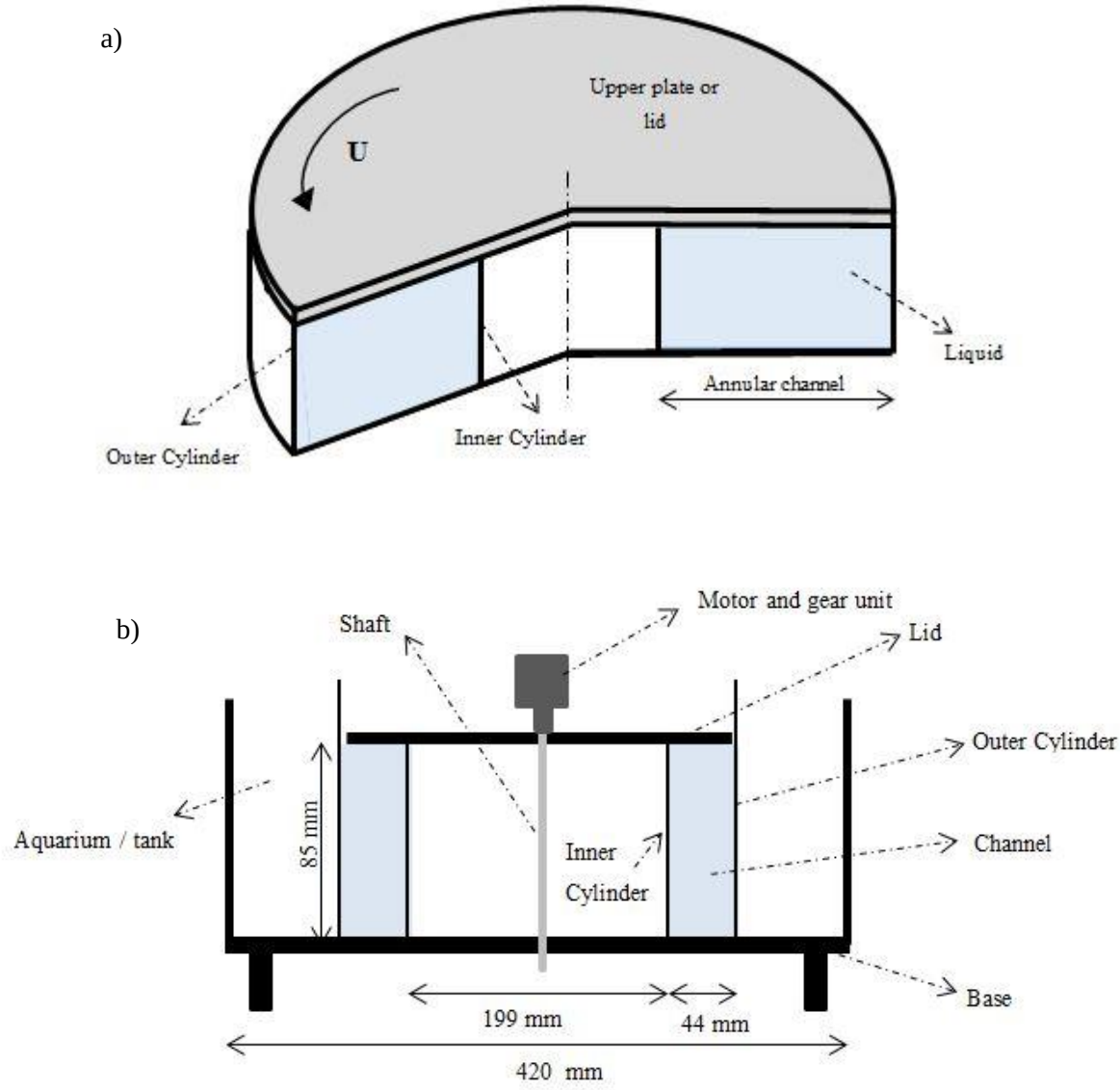

Figure 10: Sketch of the experimental setup (no scale): a) 3D sketch and b) Front view – cutting plane

The lid has a small hole in the center where the shaft bolt fits. Once the plate is placed on, the motor and the gear unit are connected, and the lid can be rotated. The motor used in the experiments is a stepper motor, 12V, 0.6A, 550 mN-m holding torque (Farnell QuickStep motor MIS231) and the gearhead is a Planetary Gearhead GPX 22 C Ø22, 2- stag,16:1-44:1 that in our case it reduces the spindle speed delivered by the motor with from 1:25. This means that if the spindle speed applied in the software is 2500 rpm the actual rotation rate of the lid is 100 rpm ± 0.2. Furthermore, an encoder ENX 16 EASY 1-1024 impulse is utilized.

The height of the inner cylinder is 100 mm and water should be added into the annular channel up to a height of 85 mm where the lid sits. It is important to note that the height of the outer cylinder is larger than the inner one to ensure that no liquid from the external aquarium can go inside the annular channel, keeping constant volume between the two cylinders, since water is poured in the external aquarium to a minimum level equal to the water level inside the channel to avoid light reflection while shooting out the laser for PIV. The rotating lid drags the fluid which in turn drags the particle bed.

The specific diameters and thickness of the cylinders and aquarium tank are shown in the graph below:

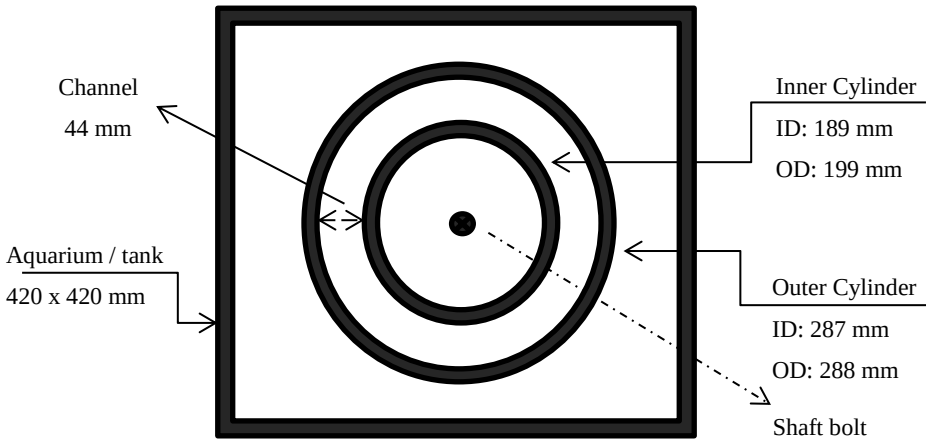

Figure 11: Simplified top view of the rotational cell without the upper plate

The present experimental set-up is different from the main classic flumes (open channels) since in this case we have a closed curve channel where centripetal force is creating a secondary complex flow. The advantage of this rotational cell is that problems associated with the supply of fluid and particles to ensure stationary and homogeneous flow condition are avoided (Charru et al., 2004). Additionally, other benefits are strict mass conservation, rotational symmetry, high spatial and temporal resolution (Betat et al., 1999).

3.2) Liquid and particle properties

The annular channel is filled with approximate 2.85 litres of deionized water (density of 0.9982 g/cm^3 at 20°c). The first trial was to use tap water but some minutes after adding it into the channel many small bubbles appeared and they were difficult to remove. Then deionized water was tried obtaining fewer bubbles and as result the last one is utilized.

The particles used are spheres of aluminium with a density of 2700 kg/m^3 that were sieved in order to reduce the size variation. Three different sizes of spheres are used in the experiments and their diameters were measured by means of photos taken with a microscope with a resolution of 0.007 mm; the median diameter, the standard deviation, the average diameter, and the spread measure (P90 minus P10) obtained from the analysis are presented below and the histograms are shown as well.

Table 1: Particles Diameter Distribution

Particle type	**Median diameter Ø [mm]**	**Standard deviation**	**Mean diameter [mm]**	**Spread Measure**	**Histogram**
Aluminium sphere	2.00	0.007	2.00	0.01	Figure 12
Aluminium sphere	1.00	0.008	0.99	0.02	Figure 13
Aluminium sphere	0.51	0.01	0.50	0.02	Figure 13

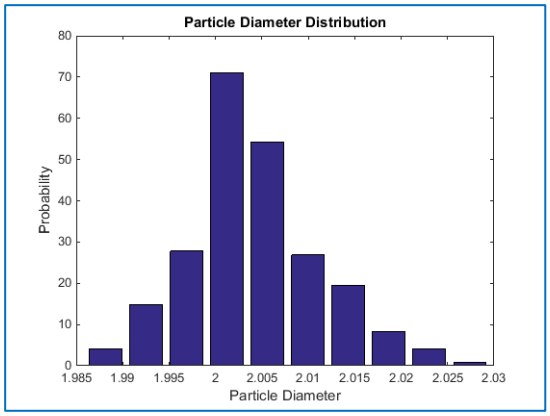

Figure 12: Particle diameter distribution (Ø 2.00 mm)

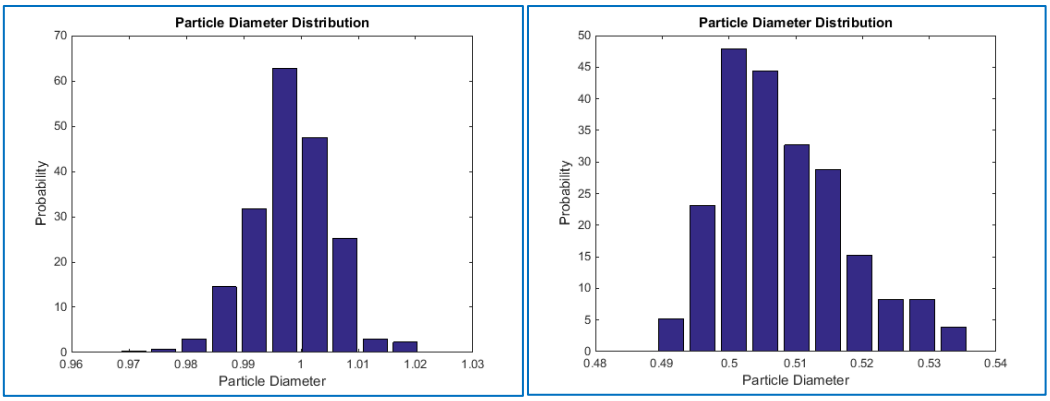

Figure 13: Particle diameter distribution: left (Ø 1 mm) & right (Ø 0.51 mm)

3.3) Measurement technique

Particle Image Velocimetry technique (PIV)

The Particle Image Velocimetry is a thoroughly used non-intrusive experimental technique carried at a laboratory which allows observing and getting various fluid variables including the vorticity, velocity in streamwise (u component) and in vertical direction (v component), velocity magnitude, among others (Cousin, Torres, Zabihian, & Panta, 2015; Khatibi, Time, & Rabenjafimanantsoa, 2016). This technique is very much used in the educational environment to study the flow dynamics. To implement this, it is necessary to have a group of components such as seeding particles, a high-speed video camera, a strobe or laser with an optical arrangement (normally cylindrical lens to convert a light beam to a line), the fluid to be investigated and a computer.

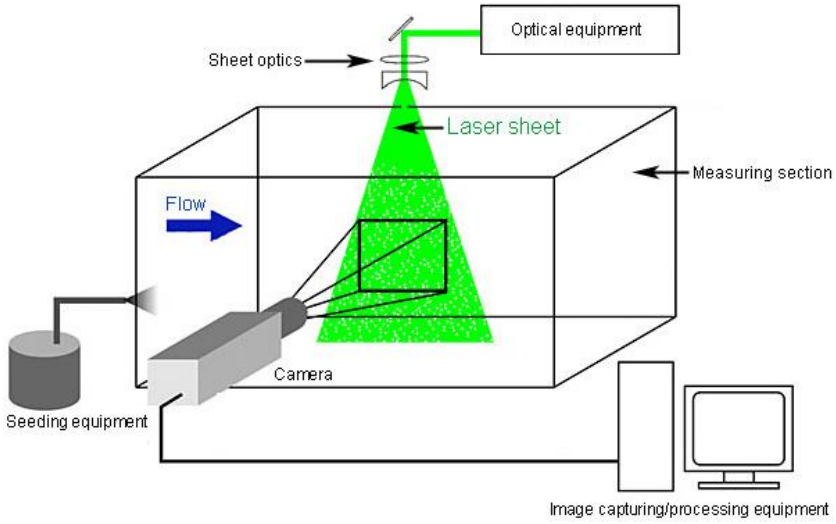

Figure 14: PIV measurement system. Modify from http://www.aero.jaxa.jp/eng/publication/magazine/sora/2012_no45/ss2012no45_01.html

The seeding particles are a very important component of the PIV system since these particles must travel along the fluid allowing to observe the nature of the flow; thus they shall match the properties of the fluid so that they are able to follow the flow without disturbing it. The idea is that these particles must have the same or approximately the same density as the fluid system where they are being used. In other words, the seeding particles should (1) exactly follow the motion of the fluid, (2) do not alter the flow or the fluid properties and (3) do not interact with each other, (Westerweel, 1997).

In short, the laser projects a sheet of light through the flowing liquid to illuminate the seeding particles in the fluid considering that these particles reflect the light with a different intensity than the fluid does and with a high-speed video camera consecutive photos are taken in a very small period of time in order to visualise flow and measure instantaneous flow velocity field. After recording at least one pair of pictures (a frame) the particle velocity that is the same as the fluid can be calculated, this is done by determining the distance that a tracer pattern has been displaced over the shooting time. In this way, it is possible to get the fluid flow velocity profile in a system after analysing the whole section created by the laser sheet. It is clear that these very imperceptible movements are almost nonvisible for the human eye and an algorithm is required in order to carry out this operation; cross-correlation algorithm is commonly used to analyse the data obtained from PIV experiments.

3.4) PIV system on the experimental set-up and procedure

In Figure 15 the PIV system installed on the experimental setup is shown. A high-speed Basler (A800-510) monochrome camera with a resolution (H x V) of 800 x 600 pixels was located pointing to the green light sheet and used to capture the seeding particles movement in two dimensions. In this case, two hundred photos (per experiment) were recorded, at a rate of 500 frames per second, and saved in the computer for further analysis. The green light sheet was generated by a 532 nm green laser (Photon DPGL-2200) which was carefully manipulated and fixed to illuminate in different positions (cases) between the outer and inner wall of the annular channel in order to visualize the flow at different depths. Finally, non-spherical but round polyamide seeding particles with a diameter range of 30 to 70 μm, density of 1.03 g/cc, refractive index 1.5 were mixed with the water to trace flow and measure the field velocity profile; these particles are microporous and strongly recommended for water flow applications (Dantec Dynamics).

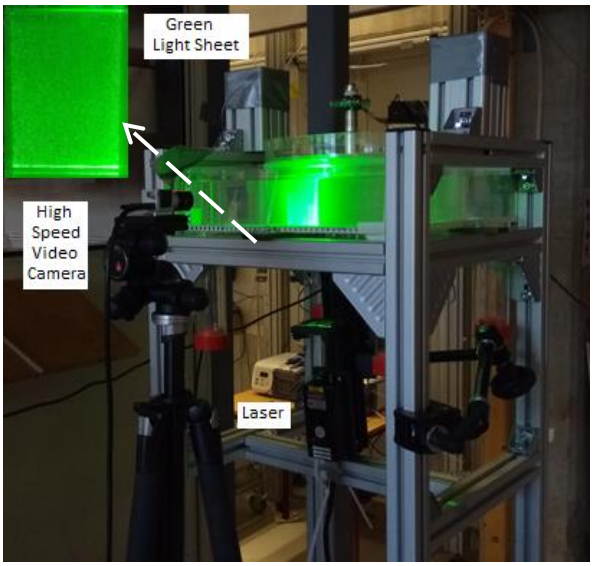

Figure 15: PIV system at UiS Multiphase laboratory

It is important to note that even though all the necessary security measures were taken into account and implemented, it was not allowed to manipulate the laser device due to the lack of previous experience and this could be very harmful to the eyes. Special thanks must be done to the supervisor Milad for helping and teaching everything related to this.

As it was mentioned before, the laser was shot in different radial positions (cases) in the annular channel in order to get data to create a 3D liquid velocity profile. Besides, for each case, data at seven different upper plate's velocity was recorded, see table 2. It is important to remember that with PIV technique we obtain image planes (2D), in other words, at each position along the radial direction (r-axis) where the light sheet is placed we can observe and calculate the flow velocity in x-direction throughout the height of the channel; the z-axis, see Figure 16.

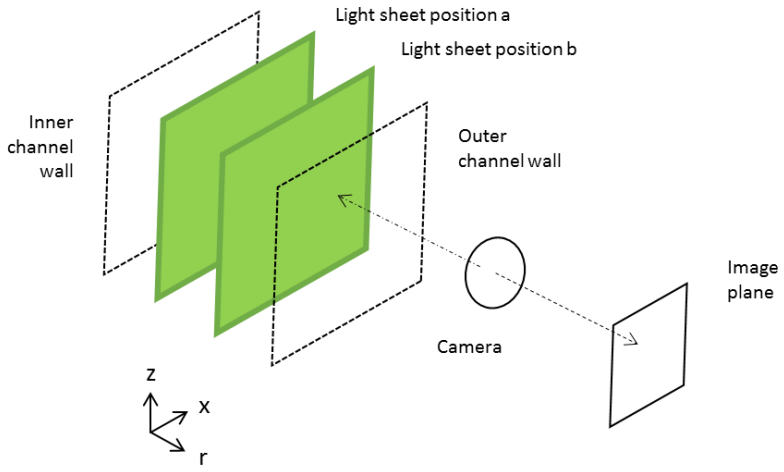

Figure 16: Schematic representation of sheet light positions

Table 2: Test matrix for 3D velocity field

		Upper plate's spindle speed [revolutions per minute]						
Position	Radial position (mm)	20 rpm	40 rpm	60 rpm	800 rpm	100 rpm	120 rpm	160 rpm
Case1	120.2	X	X	X	X	X	X	X
Case 2	136.8	X	X	X	X	X	X	X
Case 3	100.1	X	X	X	X	X	X	X
Case 4	134.0	X	X	X	X	X	X	X

The next step after recording the images for each case and all rotation speeds (rpm) was to process them. In this opportunity, the chosen program was PIVlab which is a time-resolved particle image velocimetry software programmed in MATLAB. This was selected due to its accuracy and easily understandable interface besides it has many other features apart from calculating only velocities in fluids such as data smoothing, streamlines, extensive data extraction tools, many data export feature, etc. (Thielicke & Stamhuis, 2014). Detailed and very explanatory information about this application is given in PIVlab blog and the paper mentioned just before. The present PIV analysis is divided into three main steps; image pre-processing, image evaluation and post-processing. The first one is to improve the images and for this case, a rectangle was created in order to choose the centremost part of the pictures avoiding the edges where flow was not totally perpendicular to the camera lens.

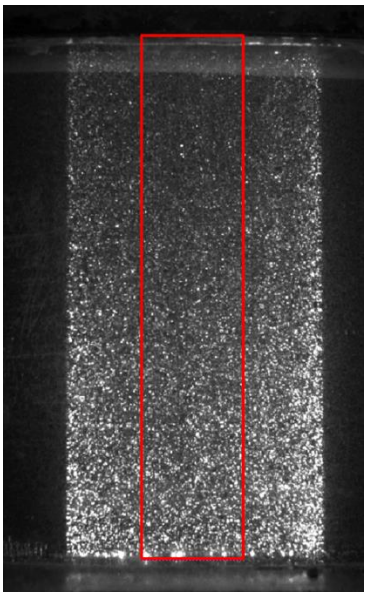

Figure 17: Image for digital PIV analysis

Second, to evaluate the images the correlation matrix in the frequency domain (discrete Fourier transform, DFT) was chosen instead of the direct cross-correlation to avoid its computational cost drawback and it was done through multiple passes (small size of sub-images), in total 3 passes were established; 64 X 32 pixels, 32 X 16 pixels and 16 X 8 pixels, respectively. "These sizes were intended to have a very low vector resolution ("vector per frame"). The displacement data of pass one was used to balance the interrogation area in the pass two what minimize the loss of information as a result of background noise in correlation matrix and increasing the dynamic velocity range and spatial resolution in the final vector map" (Khatibi, Time, & Rabenjafimanantsoa, 2016).

Finally, in the last step, the outliers were eliminated and the calculated averaged flow velocity of all frames along the column of water (from bottom to top in the channel) was extracted and saved as an ASCII file. These files were imported to a Matlab code which was created to build up the 3D liquid flow velocity profile presented in the annular channel. The respective code is added as an annex.

3.5) Equipment and experimental setup for the experiments with particles

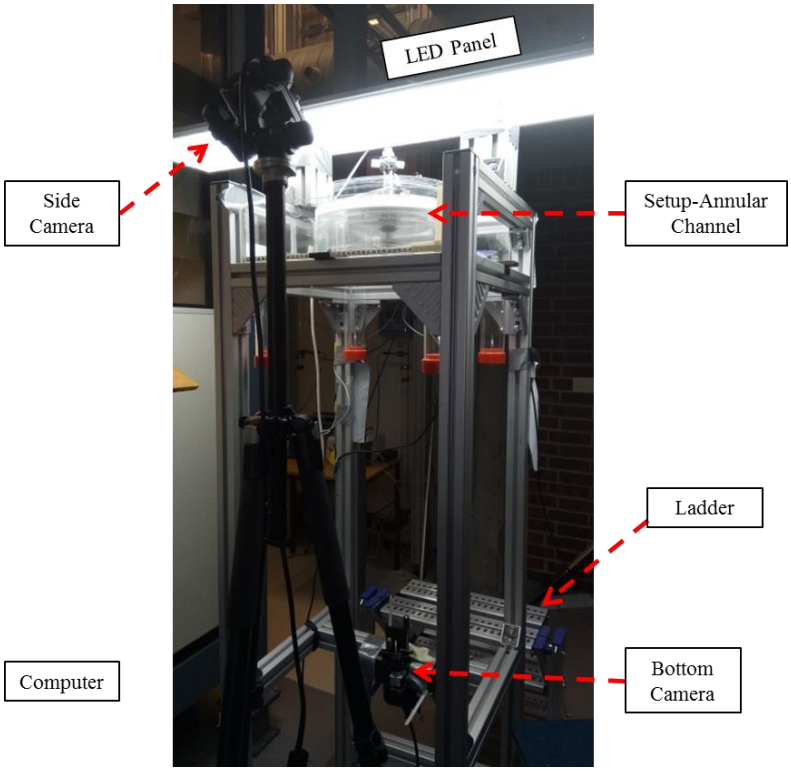

Figure 18: Equipment for particles experiments at UiS Multiphase laboratory

Figure 18 displays the total equipment used during the experiments with particles. This is quite similar to the system used for PIV described before. In this case, the laser is replaced with a LED panel which illuminates the particles otherwise fully black pictures are captured with the side camera.

This panel is placed at the top of the metallic structure. On the other hand, two cameras are used; the bottom and side camera. The latter is a high-speed Basler (A800-510) monochrome camera with a resolution (H x V) of 800 x 600 pixels and the first one is a high-speed Basler (A800-510) colour camera with a resolution (H x V) of 800 x 600 pixels. These two cameras are connected to a computer where the recorded pictures are saved for later analysis. A top camera pointing from above the setup is not installed since the upper plate is not totally transparent. Furthermore, in order to be able to manipulate the upper plate, fill the annular channel either with water and/or particles and to observe the phenomena during the runs the ladder is necessary.

Chapter 4

4) Results and discussion

4.1) PIV Results-Analysis

For each spindle speed of the lid at the different radial positions, the flow velocity profile was plotted. The first result obtained was for the lowermost rotation velocity (20 rpm) and the gotten outcome was strange at first sight (see Figure 20). We were expecting that for this case, the simplest one (only water), the main fluid flow were azimuthal and close to plane Couette flow where the liquid velocity decreases linearly from the maximum value at the lid to zero at the bottom.

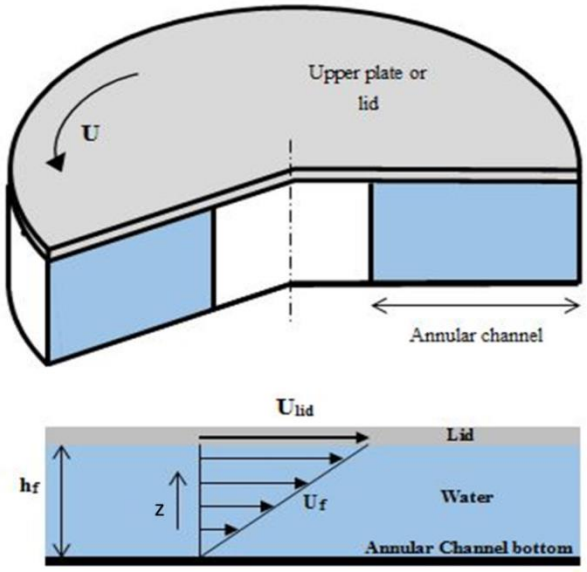

Figure 19: Sketch of expected plane Couette flow profile

With the fluid/liquid velocity equal to $U_f = \gamma * y$, where $\gamma = U_{lid}/h_f$ is the shear rate. Next, the result obtained with the digital PIV analysis for the case 1 at 20 RPM lid rotation is:

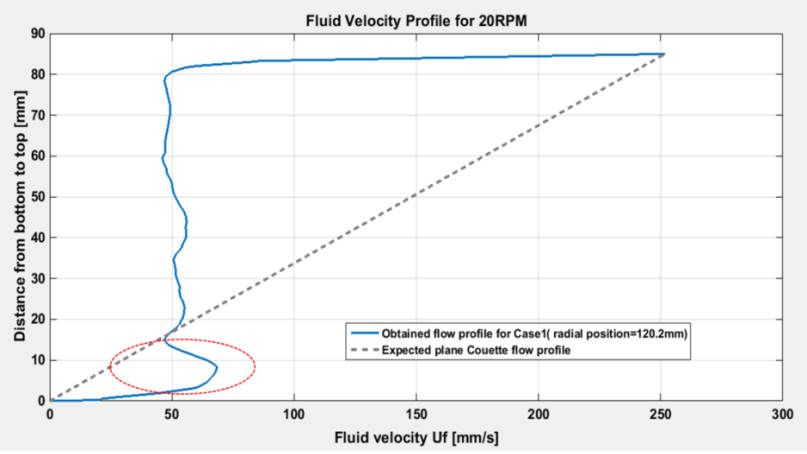

Figure 20: Liquid velocity profile for 20 RPM, case 1.

The increase of the liquid velocity (peak indicated on the graph) near the bottom of the channel led us to think that the PIV analysis was somehow not correctly carried out. Therefore the laser light sheet alignment and remaining components were double checked before running again the experiment and similar trend were obtained. Now, let us present the final result obtained for the rotation speed of 20 rpm and 80 rpm which illustrate the tendency and behaviour of the liquid velocity for the remaining plates speed.

Table 3: Reference data for 3D fluid profile at 20 RPM and 80 RPM

Lid rotation speed		20 RPM	80 RPM
Position	Radial position [mm]	Angular velocity W [rad/s]	Angular velocity W [rad/s]
Case 1 (blue line)	120.2	2.09	8.37
Case 2 (orange line)	136.8	2.09	8.37
Case 3 (yellow line)	100.1	2.09	8.37
Case 4 (purple line)	134.0	2.09	8.37

In the graph below on the x-axis is the radial position which increases from left to right; being left and right the inner (r = 99.5 mm) and outer (r =143.5 mm) wall of the channel, respectively. Second, on the y-axis is the height of the annular channel which goes from zero at the bottom to 85 mm at the top where the lid is dragging the liquid and the liquid velocity is on the z-axis. The dotted lines (case 5 and case 6) are interpolated values. On the other hand, the second type of graph is a surface plot where all the coordinates are still the same as the described just before but the radius increases from right to left; being right and left the inner and the outer radius respectively.

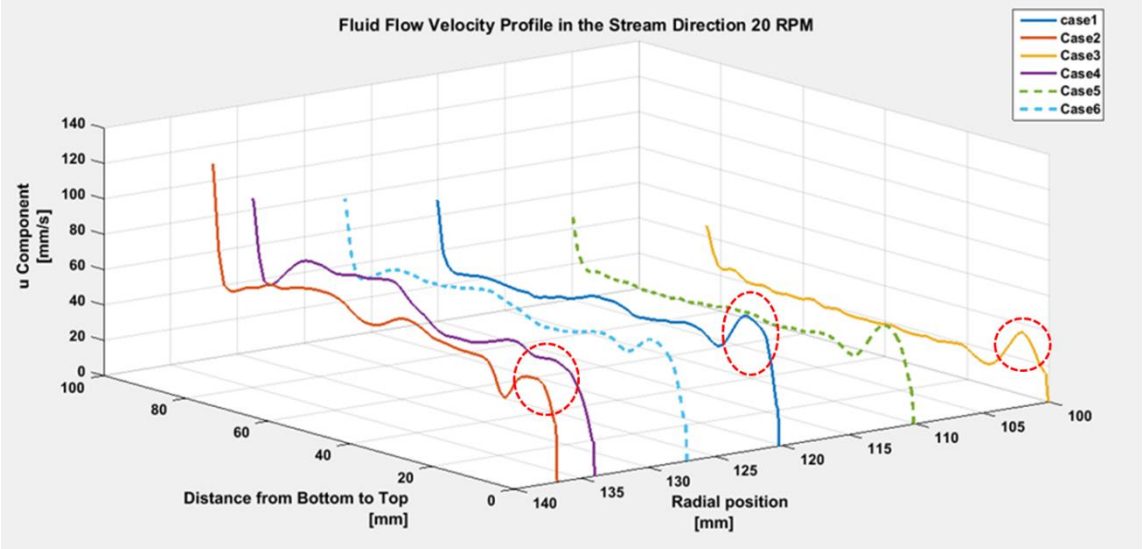

Figure 21: 3D Liquid velocity profile in the annular channel at 20 rpm

From the obtained graph for all radial positions we can observe the following important facts:

1. The lines at each different radial position describe similar trends varying only in magnitude. Here it is important to add that images for each position (radial distance) were recorded in different days and also it was necessary to move and readjust the laser device and the camera what naturally implies some small lag. This can explain the small changes in shape among the lines.

2. The liquid velocity at the top of the channel increases as the radial position increases, (red arrow) which it is in accordance with the expected radial velocity profile in the annulus.

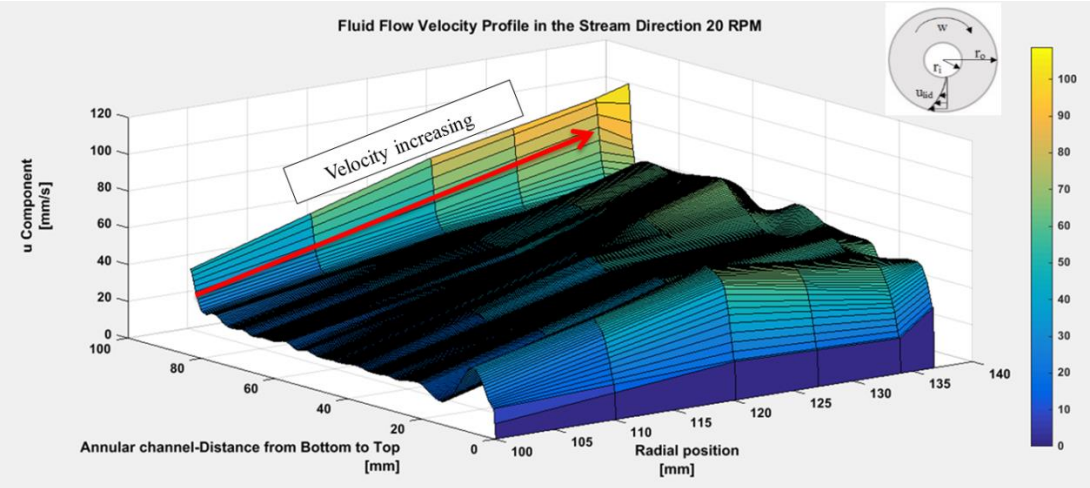

Figure 22: 3D surface plot of the Liquid velocity profile for 20 RPM

3. While running the PIV experiment and recording the images the presence of a layer of seeding particles (liquid) located close to the bottom of the channel that moved faster than the upper fluid in the middle part along the height of the annulus was clearly seen. This situation was later confirmed in the 3D plots for each case and position (see Figure 21, red dotted circumference). To answer this extra experiment was carried out. In this case the light sheet was shot in a diagonal direction going from the inner wall to the outer wall of the channel as it can be seen in the image below. It is also shown on the figure the streamlines of the flow which are obtained by means of PIVlab. This makes it easier to appreciate that the rapid increase of the liquid velocity near the bottom is due to the action of the secondary flow that goes inwards at the bottom of the channel giving to the fluid at that depth and in direction of the stream a kind of push. In other words, the seeding particles that are moving at radial position b then due to the action of the secondary flow are moved inwards to a radial position a, with b>a, so they come with a higher velocity since velocity at b is larger than velocity at a. Hence this situation is kept in a continuous way and as a result the fluid layer with high velocity is created.

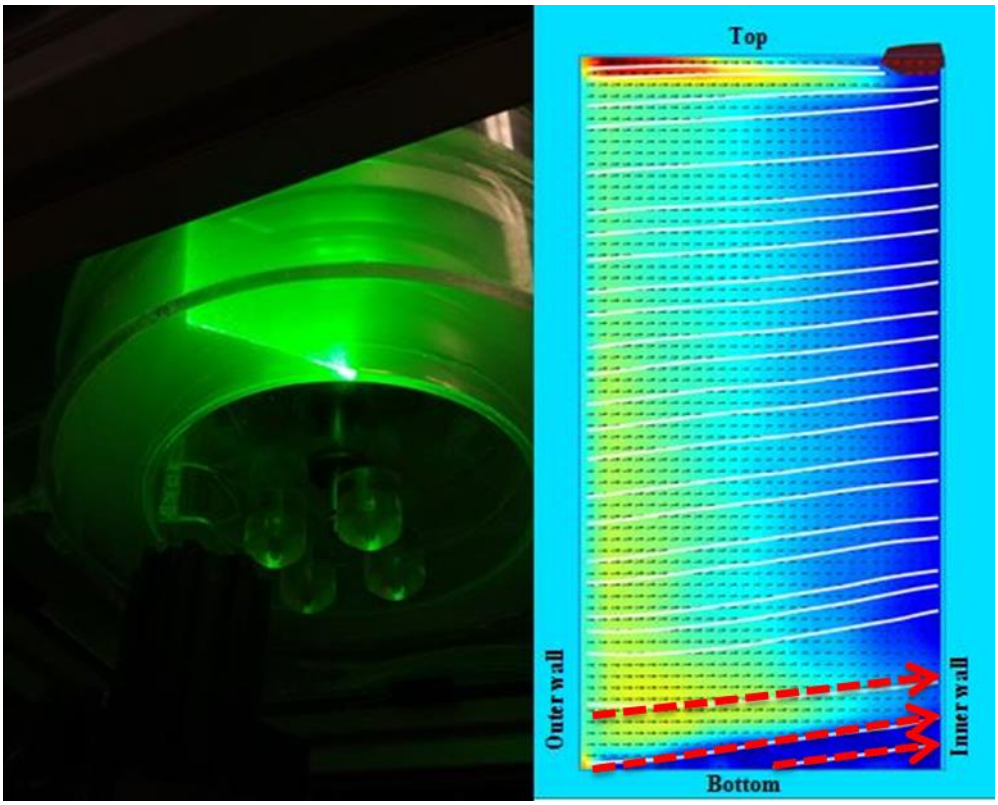

Figure 23: Light sheet shot in diagonal direction and flow streamlines

4. In the same way, in Figure 24 we can observe the effect of the secondary flow in the liquid velocity in the stream direction as it was concluded before but now here it is easier to appreciate how this effect is larger closer to the inner wall. In other words, the peak

velocity near the bottom, pointed by the dotted line, is much larger close to the inner wall. And when we are close to the outer channel wall the peak almost vanished and a smoother curve is seen. So the outward "return" flow is much more spread out and more difficutl to see.

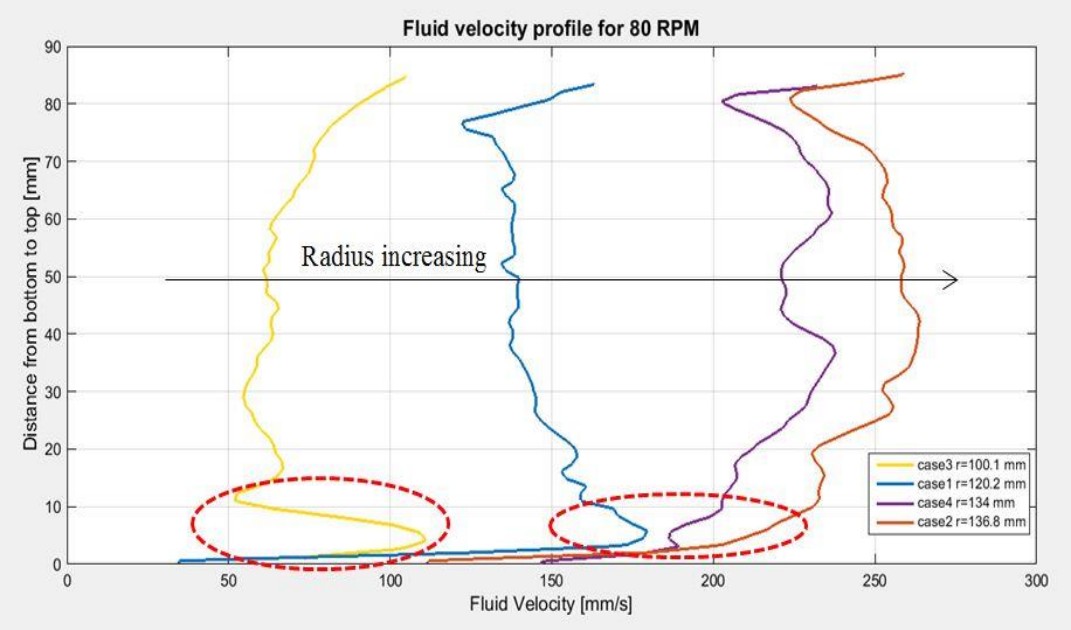

Figure 24: 2D Liquid velocity profile for 80 RPM, for different radial positions

The 3D liquid velocity profiles for others rpm are shown in the annex A and as it was mentioned before, the remaining graphs follow the same trend.

4.2) Complementary study of the fluid flow profile with "big neutral particles"

The objective is to complement the PIV study of the flow profile in the annular channel. In this case, we want to use big "neutral density" particles such that they can be observed with a naked eye and we can track (also record) the path-lines that these particles follow. The prediction is that if these big neutral particles can exactly follow the motion of the fluid, we can easier observe the effect of the secondary flow in the annular channel; more specifically observe the flow in the transversal direction.

Then, by trial and error particles made of glass (no solid) were filled with dyed deionized water and sealed with silicone. By filling a particle and test it in water; using a syringe fluid was removed or added, the particle was sealed and tested again. Anyway, after many trials, it was not possible to make particles staying neutrally buoyant in the middle of the fluid, see Figure C - 3. They either floated or went to the bottom but very slowly. The next step was to run the experiment using these particles.

Different experiments were conducted and here two specific cases are presented; Case 1: a glass neutral particle located at bottom of the annular channel and case 2: two glass neutral particles (1 at the bottom and 1 at the top in contact with the lid). The lid rotation speed, ranged from 0 to 11000 RPM.

4.2.1) Two glass neutral particles at 120RPM

In this graph below the path-lines at which the particles at the bottom and top follow are shown. The color dashed lines represent the approximate radial positions for each particle along the annulus. What it is interesting here is that the particle at bottom mostly moves following a constant radial position. It was expected that this particle moves towards the inner wall and collides with this, as a result of the effect of the secondary flow at the bottom.

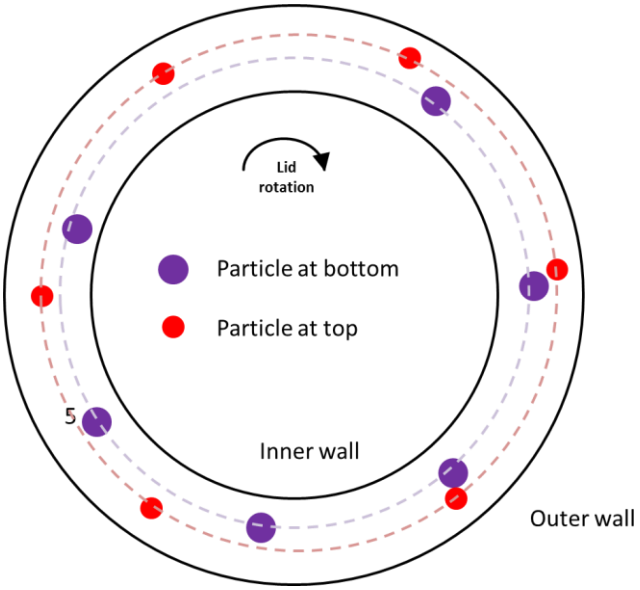

Figure 25: Radial moving position of a "glass neutral particle" at top and at bottom for 120 RPM. Particles were visually/manually tracked.

The particle moving at the top in contact with the lid moves faster than the particles at the bottom since the lid is practically dragging that particle. While at the bottom is the fluid which drags the particle which slides over the bottom assembly.

4.2.2) Motion-Radial position at different RPM's for a glass particle at bottom

For this case only one glass neutral particle was used, this one was located at the bottom and close to the outer wall. The upper plate spindle speed was increased from zero to 10000 RPM and many frames were recorded at different rates (10 fps, 20 fps, 100 fps...). The end result is the figure below where the glass particle radial positions in the annular channel at different RPMs are summarized.

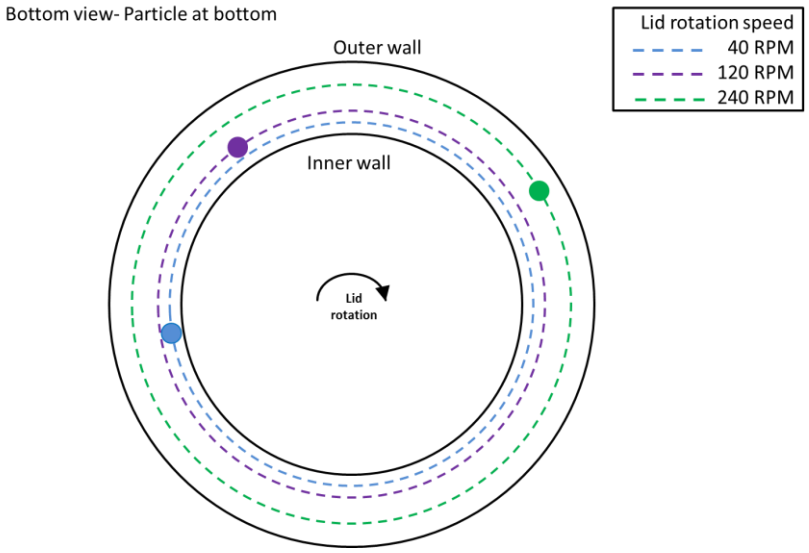

Figure 26: Radial moving position of a "glass neutral particle" at bottom varying the lid rotation speed. Particle was visually/manually tracked.

The first observation is that the threshold of motion for this particular particle is much less than for the aluminium particles since it has a larger area exposed to the flow, and thus a stronger drag force. This started to move around 40 RPM.

On the other hand, the "strangest" observation is that for the particle at bottom; at low RPM it moved following a constant radius close around the inner wall (dotted blue circle in the graph) but when increasing the lid rotation speed the particle moved again following a constant radius but further from the inner wall following (dotted green circle in the graph). This is strange since it was expected that the particle moved closer to inner wall as the angular speed increases and that at some point the particle was lifted and directed toward the top and then outwards; following more or less the red arrows in Figure 2. However, this didn't happen, the possible driver of this can be as follows (effects on the flow due to bend),(Ben Crosby, Fall 2006):

- The flow experiences a radial acceleration around the bend. The centrifugal force acts in proportion to the mean velocity:

$$\frac{\rho \overline{u_f}^2}{r_c}$$

  where r_c is a minimum at the bend apex, so acceleration is greatest there

- The secondary flow arises because the pressure gradient cannot balance the centrifugal force.

- So water is driven across the channel by the radial acceleration until enough water piles up of the outer bank to produce a "super-elevation" sufficient to create a pressure gradient to balance the (average) centrifugal force:

$$\rho g \frac{\Delta h}{w} = \frac{\rho \overline{u_f}^2}{r_c}$$

Where Δh is the required super-elevation

Then in our set-up, there is a gap between the lid and the outer wall. As a result, when the RPM increases, the fluid goes up along the narrow gap increasing the height of the fluid at the outer most radial positions (see figures below). It is believed that this extra fluid height acts as the "super-elevation" trying to balance or diminishing the imbalance between the fluid pressure gradient and the centrifugal force.

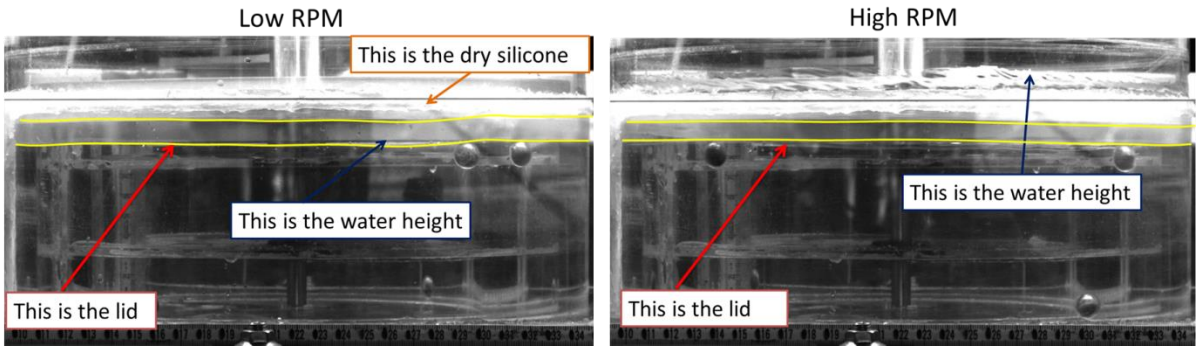

Figure 27: Side view set up with glass neutral particles at low and high rpm

Based on the previous hypothesis, it can be explained why the glass particle (located at the bottom) moves following a larger radial position as the lid rotation speed increases. This is because the imbalance is reduced as the lid rotation increase (water height at the outermost radial position increases) and this turns into a diminishing of the secondary flow strength.

At lid rotation speed of around 320 RPM; this glass particle went from the bottom to the top (lid) of the channel and kept moving at that place. In this case, the high angular velocity gives a rise to a high enough differential pressure between the top and bottom of the glass particle due to the fluid velocity gradient along the particle so this delta pressure gives rise to a lift force. For the author, this force is the responsible for lifting the particle from the bottom of the annular channel first. However, how the particle is kept in suspension and continue going up to the lid is not well understood.

Please refer to the PowerPoint file called "Neutral glass particle experiments" in which you can see some videos of what is described here.

Finally, it is possible to conclude that the glass neutral particles here used don't behave as real neutral density particle; these particles at the bottom are in fact slightly heavier than the liquid. Based

on this, new and different shapes like and size particles were used; plastic particles see Figure C - 4. The same objective as described before; to study the flow profile in the channel with big enough particles so it is possible to observe, by direct observation, they motion and path-line of the particle.

In this case the green, black and copper colored particles all time kept rolling-sliding at the bottom of the annular channel and based on this they are excluded from the analysis. In other words, they are far away to be neutral or semi-neutral particles. On the other hand, the spherical plastic particles (with a hole through them) at the beginning of the run, they roll at the bottom but a certain lid rotation speed they move upwards and downwards. For this reason and as can be observed in Figure C - 4 that one of the particles is floating and the other is resting at the bottom of the vessel it is possible to conclude that these plastic spherical particles are more neutral than the glass ones.

The experimental results present here, in this case, correspond to the runs for a single spherical plastic particle located at the bottom of the annular channel, starting from zero lid rotation speed to 8000 rpm.

- In the beginning, the particle rolls around and close to inner cylinder similar to the glass particle did. However, in this case, it didn't follow a constant circular path-line. The particle moved toward the inner wall colliding with this and then went to a further radial position moving at a pretty much constant radius path along the channel until it came again towards the inner wall. It can be said that the secondary flow is the reason for which the particle goes towards the inner wall. Furthermore, as the lid rotation speed increases the radial position at which the particle goes after the collision with the inner wall also increases that is that the particle goes closer to the outer wall.
- Once the lid rotation speed is large enough so the fluid is able to lift the particle some distance above the bottom wall, the particle is lifted some millimeters while rotation around the channel and fall down, this more or less happens when the particle is a radial position equal to the middle point of the channel what means that here we have the same situation as with the glass particle. This means, that the particle doesn't go very close to the inner wall and after is lifted.
- Approximately at a lid rotation speed of 240 rpm, the particle went from the bottom (the midpoint of the channel) to the top (lid) of the channel while rotating around. Once the particle is below the lid it is dragged towards the outer wall and rotates for a while until it goes downwards in a diagonal direction toward the midpoint of the annular at the bottom. Then this kind of movement is repeated. Again, why the particle did not go very close towards the inner wall and then ascended (as expected), it is not clear. The reason for this phenomenon is not well understood. In other words, why this particle goes upward at the midpoint of the channel-width is not well understood.

To close this section, these experiments were run at the end of the thesis based on an idea that came up from the revision of this report. The most important factor here is the neutral object; different particle size, material, and shape were used. We considered that the glass with dyed water and air utilized here behaves as semi-neutral and because of this the experiments didn't result in better outcomes. On the other hand, the spherical plastic particle tends to be more as a real neutral particle and because of this; it was possible to observe the particle going from the bottom to the top of the channel and returning again to the bottom. However, there are still the questions to resolve that can be addressed for a future investigation. To sum up there seem to be effects relate both to size and density of the particles, but due to the complex flow field, it is difficult to draw final conclusions of the combined effects.

4.3) Particles Flow Experimental Results

Before going into the description of experimental results, it is important to understand some of the nomenclature here used.

4.3.1) Important Nomenclature

Bed-width: width of the base of the bed and the obtained deposition geometry, this is easily observed with the bottom view camera, see figure below.

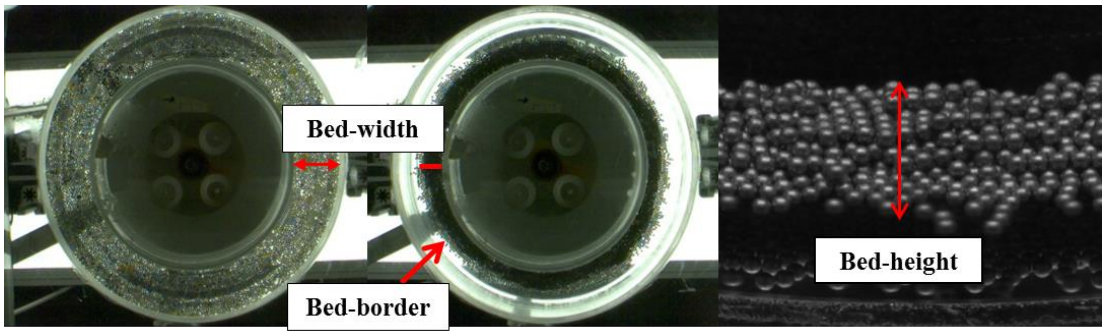

Figure 28: Nomenclature: Bed-width & Bed-height

Bed-border/perimeter: the most external part of the bed across the annular channel.

Bed-thickness: height of the bed from the base of the bed (set up bottom) top the topmost particles along the height of the annular channel, seeing with the side view camera, see figure below.

After presenting the short nomenclature, we are ready to going further into the experimental results. The temporal evolution of bed-width, bed-thickness, bed erosion and particle deposition are displayed.

4.4) Single size particles – 2 mm

In this part, plots & images and detailed description of one of the experiments is presented. The idea is to describe the best possible outcomes from one of the different runs carried out with particles and deionised water.

The parameters, of the here presented case, are the following:

- Single size particles; diameter equal to 2 mm
- Aluminium spheres 100 grams in total.
- Deionised water.
- Plane bed

The first step was to fill the annular channel with the deionised water and wait for some minutes to see if bubbles appear. Small bubbles occurred often but they were manually removed. The 2 mm particles were then added and manually distributed in such a way that they totally filled the width of the annular channel (from the inner to the outer wall) in order to obtain a plane bed. In this case, a thin and plane bed with a height of one particle diameter with few particles above this was generated, see figure below.

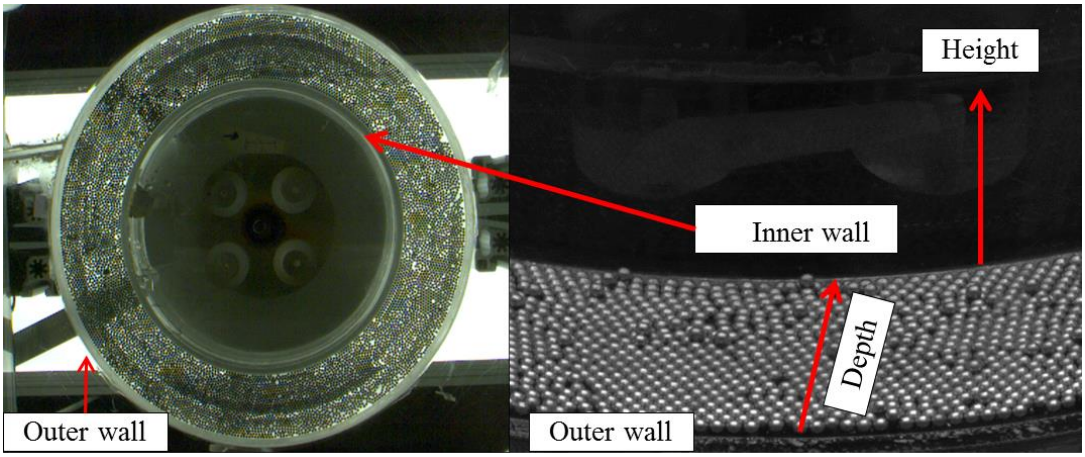

Figure 29: Bottom and side view of the manually distributed initial bed for 2 mm particles diameter

The next step was to find at which upper plate's angular speed particle motion starts; going from 20 rpm to 160 rpm in steps of 20. For each rotational speed pictures were recorded at different times (minutes) then if for a given RPM no particle motion was observed during the first 30 minutes the speed was increased. The results of the observation are summarized in the table below.

Table 4: 2 mm particle initial motion

Angular Speed (RPM)	Results
20	No particle motion
40	No particle motion
60	Some few particles started to vibrate/shake however no particle motion is observed
80	More particles are shaking and at the beginning, few particles in the bed surface sporadically rolled/slid short distances. This upper plate's spinning value is the threshold of particle motion.

Since below 80-rpm angular speed particles do not move or only shake in the same position and at 80-rpm movements are sporadic, the upper plate's spinning used for the experiments must be higher in order to start motion. In this case outcomes for the 120 rpm lid rotation speed are going to be displayed.

4.4.1) Erosion of particles at initial bed and accumulation on the bed surface

First of all, let´s take a look at the erosion process of the particles forming the manually created bed. In this case, the bed erosion starts from the outer most particles in the radial direction, this means with the particles close to the outer wall. In some positions around the outer most radius, small particle free spaces are seen to be formed, see Figure 30, red dashed circles. It is believed that the secondary flow acts as the gravitational force but in radial direction compacting and rearranging the original bed packing particles hence those small free spaces are generated (yellow arrows). In the following analysis, particles were tracked visually / manually to determine the motion. An automatic tracking algorithm was nearly impossible to construct, due to the problem of identifying and discriminating individual particles.

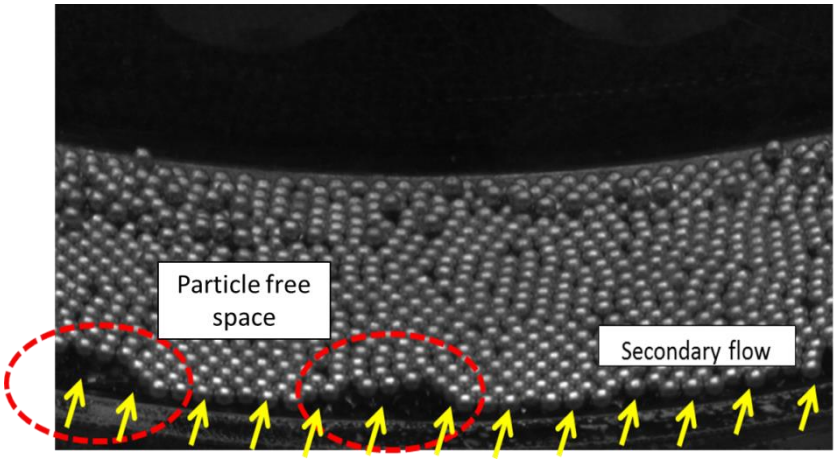

Figure 30: Graphical representation of small particle free spaces and the secondary flow, frontal view.

Once a big enough particle free space is created, the flow is able to move the particles by sliding o rolling from the tail of the free space towards the front in the flow direction; see Figure 31. These particles collide with the particles in the front; losing kinetic energy, some of them may stop and others may overcome the section going up to the surface bed or make particles in the front to jump to the bed surface due to the collision. Also, the flow is able to drag the particles at the particle-free space´s tail over the other particles.

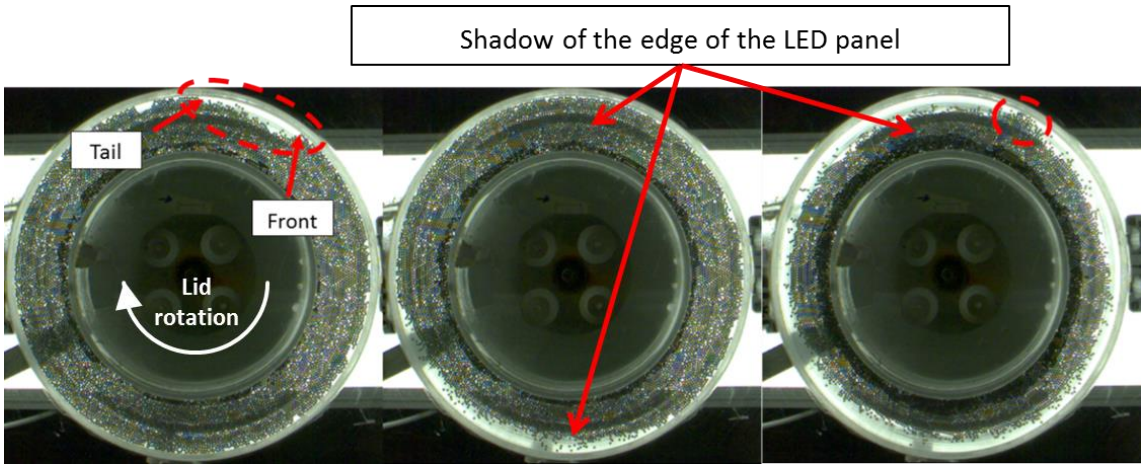

Figure 31: Temporal particle free space evolution - erosion process of the initial bed.

The figure above represents the temporal evolution of the called particle free space where capture time increases from left to right. The particle free space continues growing and would seem that it moves around the annular channel in opposite direction of the flow (flow direction: clockwise direction) but in reality as particles are eroded from the free-particle space's tail & border, some of them accumulate at the front, then the particle free space is being sealed at the front and growing at the tail. This continues until the tail reaches the front resulting in a complete, like ring shape, free space. This is the erosion process seeing from the bottom view but what about the side view.

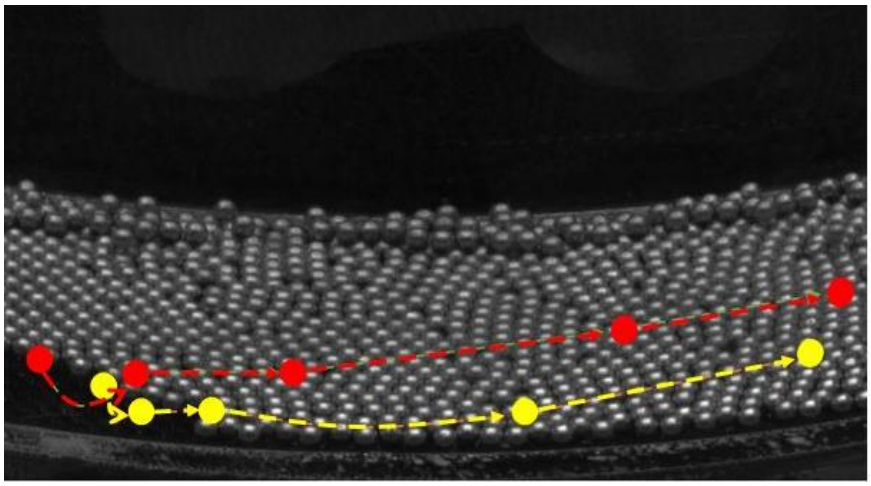

Figure 32: Particles in the bed climbing to the bed surface, 2 mm particles at 120 rpm. Particle motion was tracked visually / manually as explained in the text.

As mentioned, once a big enough particle free space appears particles move by rolling and/or sliding, arriving at the free particle space's front where due to the action of the fluid forces can overcome this section and going to the bed surface. Figure 32 displays the side view of the here presented case; 2 particles (red and yellow) were tracked through time showing their paths.

4.4.2) Temporal bed-width evolution

In this part, we address the temporal bed-width evolution of the manually established flat bed at 120 rpm. Recorded pictures from the bottom camera are used in order to show how the bed-width is changing in time from time zero (initial state) to time when the system achieves a fully developed state. The initial idea was to capture the pictures every 5 or 10 minutes however as it can be seen in the figure below, this couldn't be followed since important changes can occur in a matter of few minutes or seconds. To determine the optimum parameters for capturing the pictures two calibration experiments were first carried out. From these it was concluded that a rate of 200 frames per second good quality pictures are obtained, for a much higher rate particles look like ellipses and for fewer frames particles looked blurry.

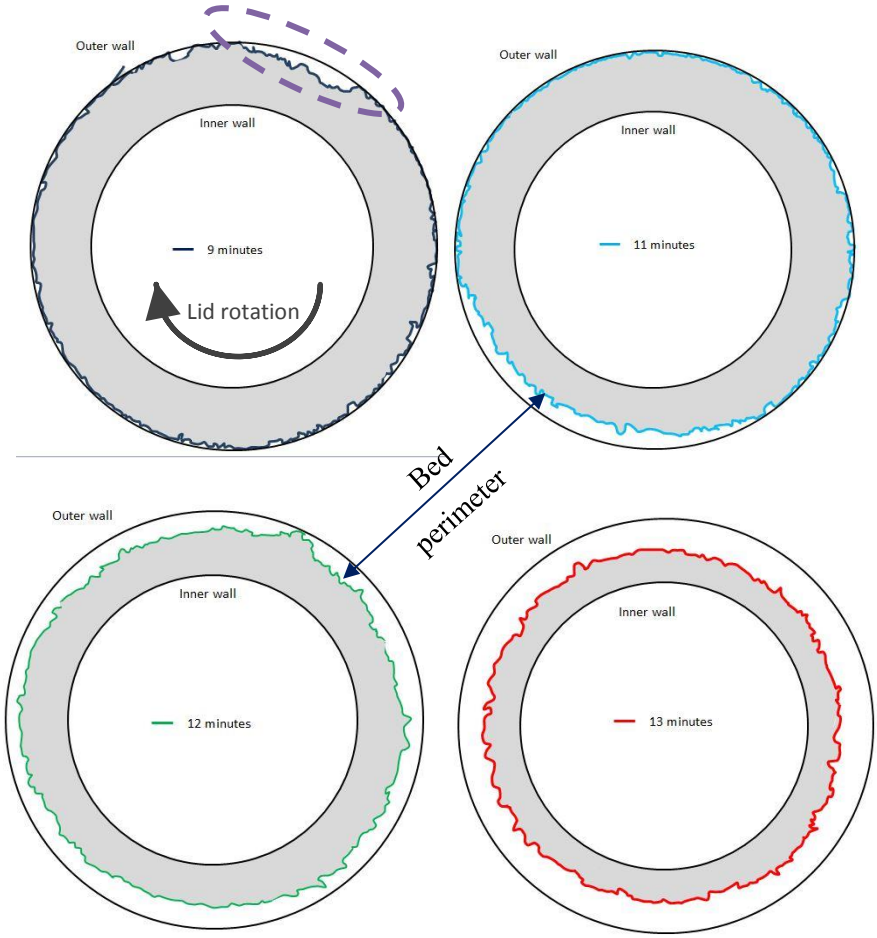

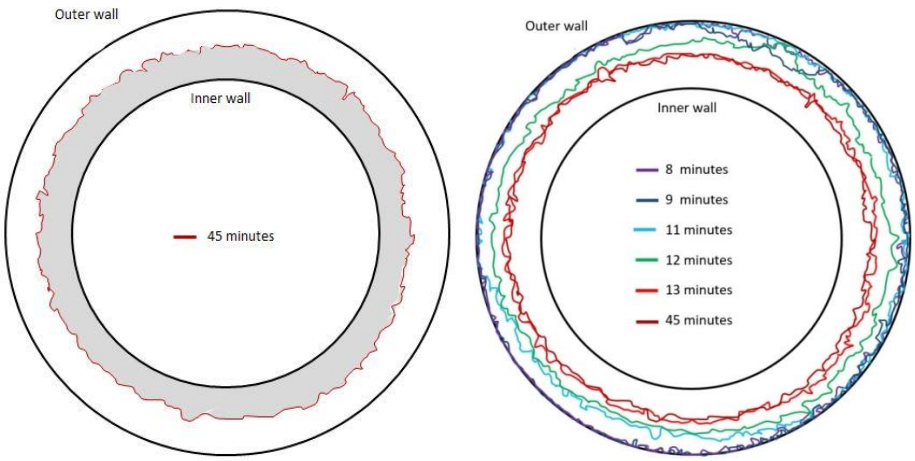

Figure 33: Temporal bed-width evolution for 2 mm particles diameter at 120-rpm. The shaded gray zone represents the particles and the color line represents the bed perimeter. Lid rotation: clockwise. Also here visual / manual tracking of interfaces was used to avoid ambiguities.

At a constant angular speed of 120 rpm, the bed-width varies strongly after some minutes (it is reduced by 11 particle diameters at time 13 minutes). It is observed that certain amount of time (8 minutes) is necessary for the flow to start eroding the bed (first layer) and once this moment is achieved, the particles in the bed perimeter are very fast removed and accumulated at the bed surface.

During the transition period a big particle free space (yellow dotted line) is formed as mentioned. This grows over time until a completely free space between the bed perimeter and the outer wall is achieved; please see the blue and green line in the figure above. In addition, it is shown that the system achieved a developed state where the perimeter remains almost the same with time; bed-width at minutes 13 and 45 remains almost invariable. At this time, a continuous ring of moving bed load is generated.

4.4.3) Temporal bed-thickness evolution

In this section, we address the temporal bed-thickness evolution of the manually established flat bed. The procedure followed is the same as for the temporal bed-width evolution but now we analyze the pictures recorded with the side view camera. The camera was set in such a way that it is possible to have a two dimensions notion; height and depth in the radial direction (width), see Figure 29.

In this case, it was not possible to have a wider image or pictures of the whole setup and the particles because since it is a thin layer (1 particle diameter height) this one was not visible when put it the camera further away. The camera used is a monochrome camera; as was described in chapter 3. In Figure 29 the plane bed and particles over this are easily appreciated. The initial bed height is equal to one particle diameter.

For a constant angular speed of 120 rpm, the bed-thickness varies strongly; increasing by 4-5 particle diameters as it is seen in figure 33 at 45 minutes. Here it is also possible to appreciate the reduction of the bed-width. It is important to mention that the bed height is larger as closer to the inner wall (see red line in the graph) and this is due to the action of the secondary flow which pulls the moving particles from the outer positions towards the inner wall and some of these particles can go to the topmost part of the bed next to the inner cylinder. Once a particle is deposited close to the inner wall it remains almost static and this is because close to the inner wall the liquid velocity is low and it is not able to drag the particle. Furthermore, the velocity gradient does not create enough differential pressure between the top of and the bottom of the particle such as this one can be lifted super-passing the submerged weight of the particles.

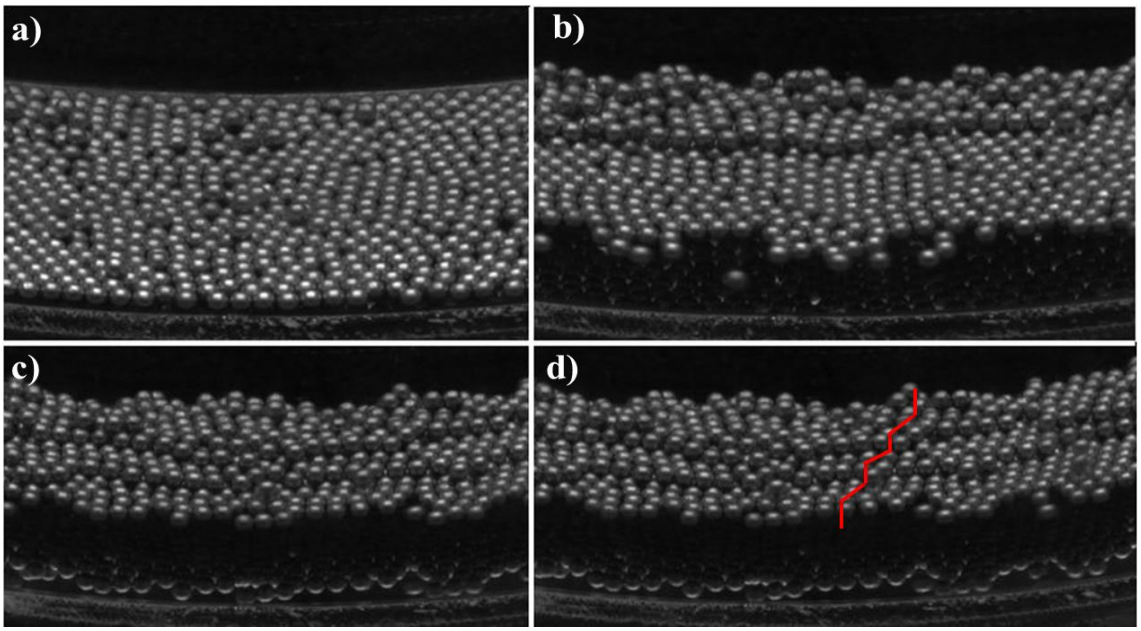

Figure 34: Side view pictures of the temporal bed-thickness evolution for the 2 mm particles at 120 rpm. a) Initial state, b) 11 min, c) 13 min, and d) 45 min. Visual tracking as earlier described.

In the Figure 34 it is also possible to see that the bed thickness did not change notoriously after 13 minutes (box c). If the two sub-frames c and d are compared to, almost the same height of the bed is visualized varying in some positions by one particle diameter. Furthermore, 3 well-defined layers result from the run giving the impression of steps. This geometry is kind of surprising because it reflects a strong structure where the secondary flow kind of mimics the gravitational force in the radial direction, keeping compact each layer.

The Figure below is a representation of the bed thickness close to the inner wall; it shows how the bed height changes with the time as a summary of what was previously described. The picture in the background is the initial state of the bed.

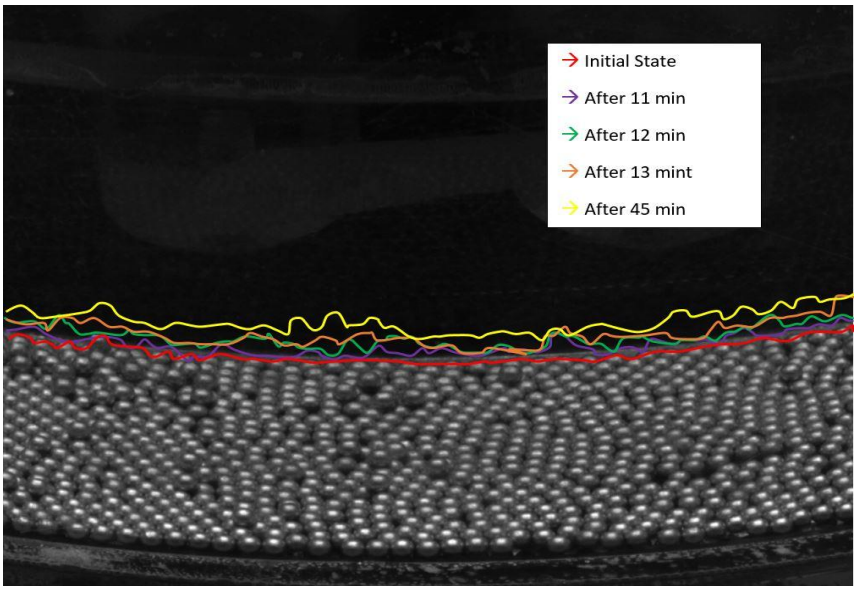

Figure 35: Summary image of the bed-thickness evolution for 2 mm particles diameter at 120rpm. Visual tracking as earlier described.

Table 5. Description of the temporal bed-thickness evolution at different times for 2 mm particles.

Time (min)	Color line	Bed thickness
0	red	The initial bed thickness close to the inner wall is about one particle diameter (red line)
11	purple	Once the experiment starts, few particles (particles on the bed surface) move towards the inner cylinder so the height of the bed increases in certain locations to 2 particle diameters and in the other point remains without any changes.
12	green	Bed height equal to 2 particle diameters along the bed and 3 particle diameters in certain locations.
13	orange	The bed height is 3 particle diameters in all locations.
45	yellow	The bed height varies from 3 to 5 particle diameters; being 4 particle diameters the most likely height.

4.4.4) Motion of individual particles

In this section, we present a study of individual particles, especially their trajectories and velocities. These quantities have been evaluated for the upper plate's angular speed of 120-rpm at developed state.

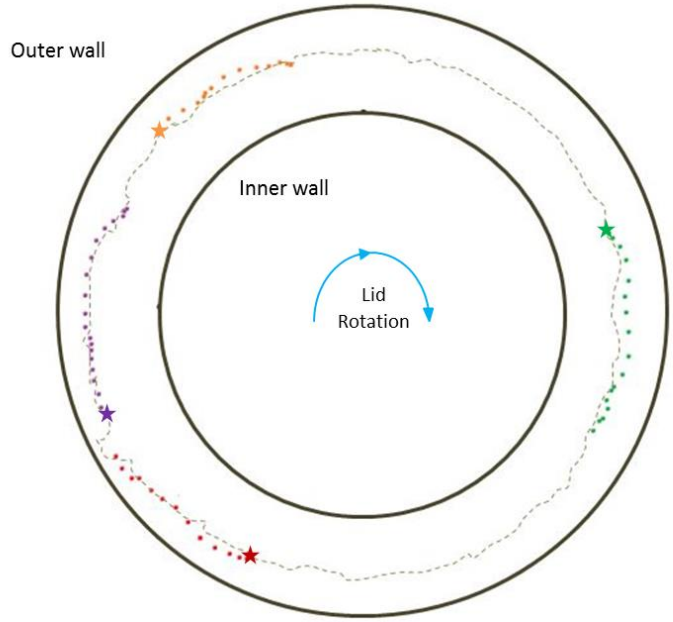

Figure 36: Four particle trajectories at fully developed state, bottom view. The lid rotation is in clockwise and each start corresponds to the beginning of the tracking. Visual tracking as earlier described.

Figure 36 shows four typical particle trajectories at the perimeter of the bed (bottom view) for the angular speed of 120 rpm. This was obtained from the recorded images sequences at 200 frames per second at developed state. The grey dotted line represents the perimeter of the bed (the bed-width) for the green tracked particle. Particles moved principally by sliding and rolling (it is very complicated to differentiate one movement from the other in this case) over the base of the setup this means that they slide or roll over the bottom of the annular channel. These particles also may stop for a while and then start again generally due to the influence of another particle or possible due to the arrangement of particles around as mentioned by (Charru et al., 2004). The trajectories presented in figure 38 correspond to the entrained particles.

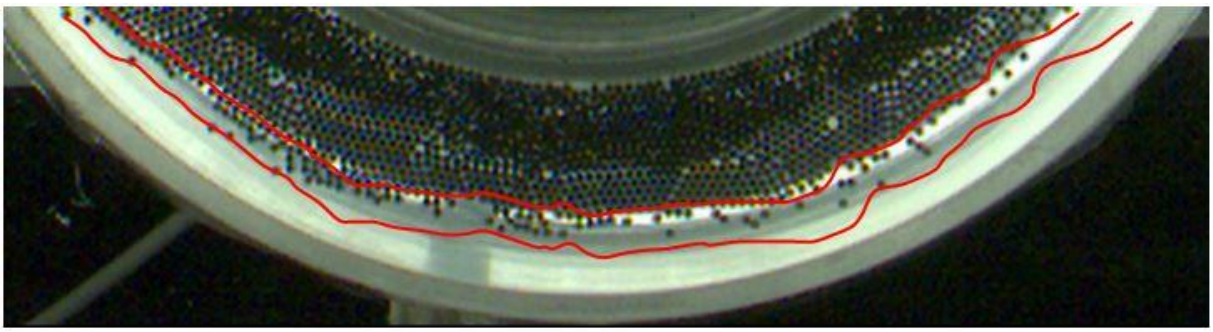

Figure 37: Particles moving layer or ring of moving particle at fully developed state for 2 mm particle diameter, 120 rpm (bottom view). Visual tracking as earlier described.

The next step is to measure the instantaneous velocity of the particles that integrates the bed-load; these are all the particles that are in motion traveling in direct contact or very close to the bed (no by suspension) (John Southard, Fall 2006). For our case, the bed-load is pointed between the two red lines in Figure 37 here called ring of moving particles or also called moving layer. It was not mentioned before but at developed state mostly particles move around the bed border, not over the bed. To carry out this operation a tracking particle velocimetry tool was going to be used however this was not feasible due to internal problems of the program's code. Many attempts were carried out to solve fix the code but it was not possible. Then, the particles were manually tracked from frame to frame-employing Matlab image tool to determine the position in pixels of the particle at frame n and the position of the same particle at frame m. Afterward, the distance in pixels that the particle moved was determined and converted to real distance with a calibration factor.

Particle position at frame $n \rightarrow (x_1, y_1)$

Particle position at frame $m \rightarrow (x_2, y_2)$ where n>m

$$Dis\tan ce = \Delta S = \sqrt{(x_2 - x_1)^2 + (y_2 - y_1)^2}$$

Since the pictures were recorded at a rate of 200 frames per second, then the time from position n to position m is calculated by:

$$Time = \Delta t = (m - n) * \frac{1}{200}$$

Finally the velocity magnitude is determined by:

$$v = \frac{dis\tan ce}{time} = \frac{\Delta S}{\Delta t}$$

The procedure to determine the instantaneous velocity of the particle in the moving layer is extremely tedious and time-consuming. Then around 110 measurements were done by using first the images from the bottom camera and after the images from the frontal camera for the angular speed 120rpm at fully developed state, these values are displayed in figure 40. The idea with this, using images from both cameras, was to provide redundancy in the procedure and avoid possible errors due to a wrong calibration factor.

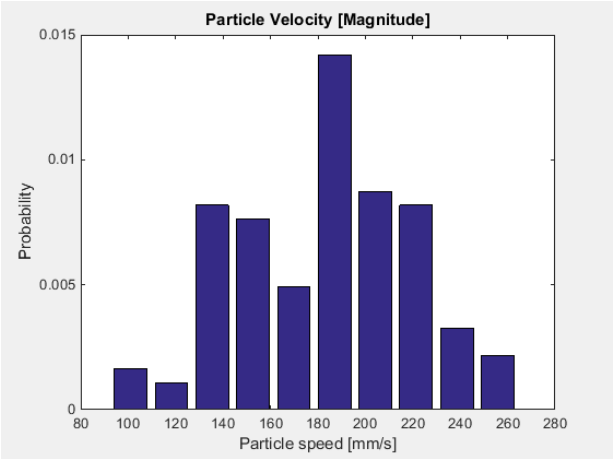

Figure 38: Histogram of particle instantaneous velocity at fully developed state for the particles in the moving layer.

The number of measures is not enough for getting a smoother histogram. Anyway, the idea with the Figure 38 is to present in a practical way the calculated particles velocities where a large variation in the speed can be observed. This velocity variation is, of course, normal and it is expected beforehand since some particles collide between them and against the bed perimeter what makes those particles to lose kinetic energy reducing the speed. Furthermore, some particles in the moving layer roll/slide around (in contact) with the bed perimeter and other particles do this a little bit far to the bed perimeter please see figure below. So those particles that roll in direct contact with the bed border have less velocity due to the extra friction between particle-particle.

Mean particle speed = 183.4 mm/s

Median particle speed = 186.8 mm/s

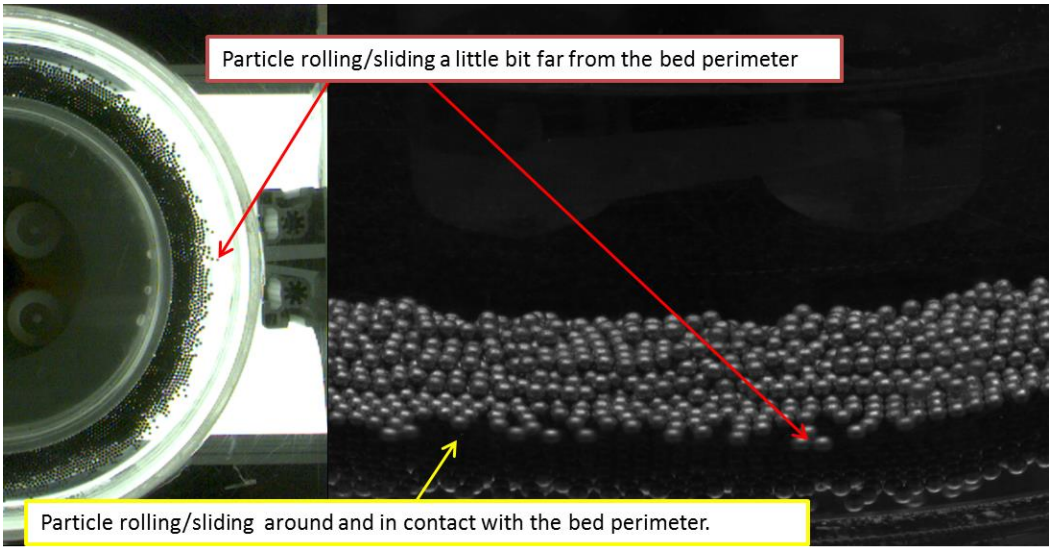

Figure 39: Particles rolling around and in contact with the stationary bed-border and particles moving a little bit far from the stationary bed.

4.4.5) Individual particle path-line during the transition and developed period

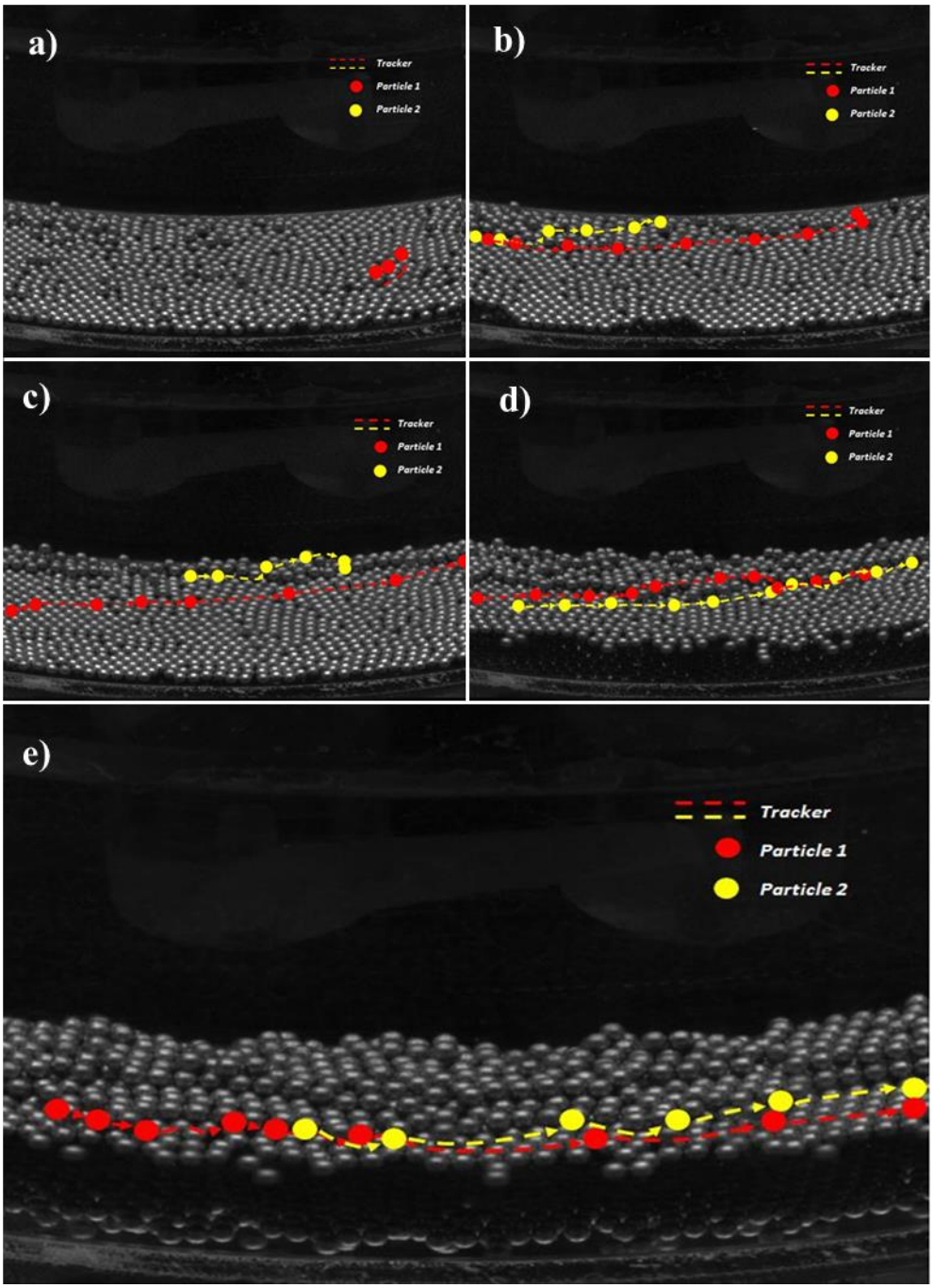

Figure 40: Individual particle motion at the second or third layer for 120 rpm at a) 25 sec, b) 8 min, c) 11 min, d) 12min & e) 13min. Visual tracking as earlier described.

Figure 40 displays the individual particle motion for the particles above the initial bed surface that is for particles moving at the second, third or fourth layer. This is composed of 5 different subpictures taken with the front camera at different times for the angular speed of 120 rpm. From this, it is possible to mention the following for each time.

- At 25 seconds (box a) the particles located initially above the bed surface start to roll short distances being principally dragged inwards. In this case, the tracked particle stop when it found a throat.

- After the first 8 minutes, more particles have been pulled to the inner wall, important to notice that those particles correspond to those that were originally at the bed surface and have more exposed are to the fluid flow, in other words, the initial bed (first layer) has not been eroded yet. In this box (b) at the begging, the two particles moved following the border of a bunch of particles but after a while the yellow particle is blocked however this one goes over (using the blocking particle as a trampoline and continue its movement until it is close to inner wall and falls in a throat). The red particle moved until it crashes with another particle and stops.

- At 11 minutes, box c, more particles on the bed surface moved but in this case, those particles come from the bed itself (first layer) that it is being eroded (not clearly seen from the front picture). The same situation as before, particles move diagonally due to the influence of the secondary flow and can either climb to the third level or be stopped by the particles that are already accumulated close to the inner wall.

Particles coming from the first layer will roll over the first layer or second layer until they hit another particle and stop or they find a room where they accommodate. The way in which a particle climbs from the second layer to the third one is that they find another particle that stands a litter more above than the others and it is used like a trampoline (see figure below) or particles come with high speed and when they collide with another particle the impact makes them go over the hit particle. The force present due to the flow at the actual lid's speed cannot lift the 2 mm diameter particles.

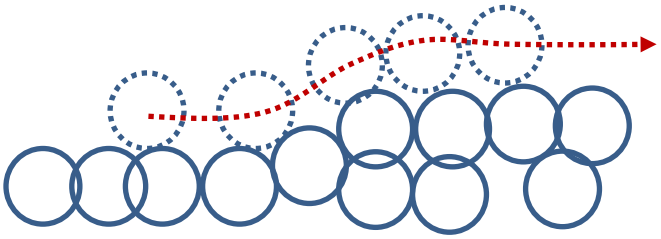

- In the box d, just one minute after, many particles accumulated close to the inner wall and it is clearly appreciated how the first layer of the bed was eroded. Regarding with particle motion, it is still pretty much the same, particles coming from the first layer move diagonally until they meet the accumulated particles. The new coming particles can climb to the third layer, stop or continue their motion around the accumulated particles. Furthermore, particles are moving around the border of the bed (first layer) by rolling and colliding with the border.

- In the last subpicture at 13 min (box d), it is seen that particles cannot move more diagonally and go close to the inner wall since the previously deposited particles create a barrier. At this time and

afterward, particles move around the border like following a constant radius of movement. Of course, sometimes some particles using another particle as a trampoline climb to the top layers. Finally, once a particle climbs to the top of the bed it mostly will stay there unless another particle affects it.

Another important fact is that the first layer is wider than the second one and the second one than the third one. However, sometimes and in some parts, the second layer becomes as wide as the first one so particles from the second layer fall feeding the first layer and they start to move.

As mentioned, this section was intended to describe the best possible the experimental results for the specific case; 2 mm particles, in other words for a single size particle. Similar experiments were run for 1 mm particles diameter where same phenomena occurred with some few differences that are going to be presented later. The next stage is to present the experimental results obtained for a mixture of particles of 1 mm and 2 mm where an interesting phenomenon occurs.

4.5) Mixture of 1 mm and 2 mm particles

The parameters of the experiment are the following:

- Mixture of particles; diameter equal to 2 mm and 1 mm.
- Aluminium spheres 200 grams in total, 100 grams of each particle size.
- Deionised water.
- Plane bed.
- Angular speed 120 RPM.

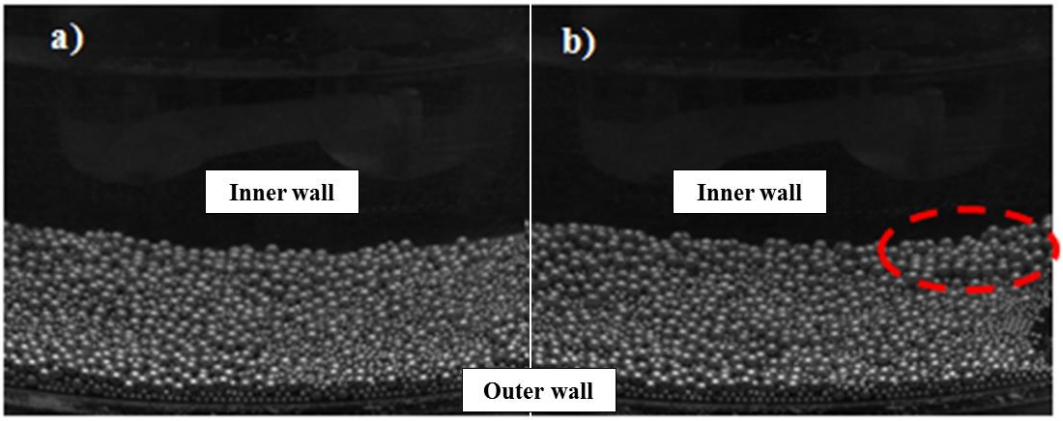

Figure 41: Manually distributed bed of non-cohesion particles of 1 and 2 mm. a) at time zero & b) at 1.5 minutes

As it is seen in the figure above the 1 mm particles are mostly located between the 2 mm particles at the bed surface and once the upper plate starts to rotate the 2 mm particles move first due to the fact that they have a more exposed area to the flow (A_f).

$$F_D = \frac{1}{2} C_D \rho_f \left(\bar{u}\right)^2 A_f$$

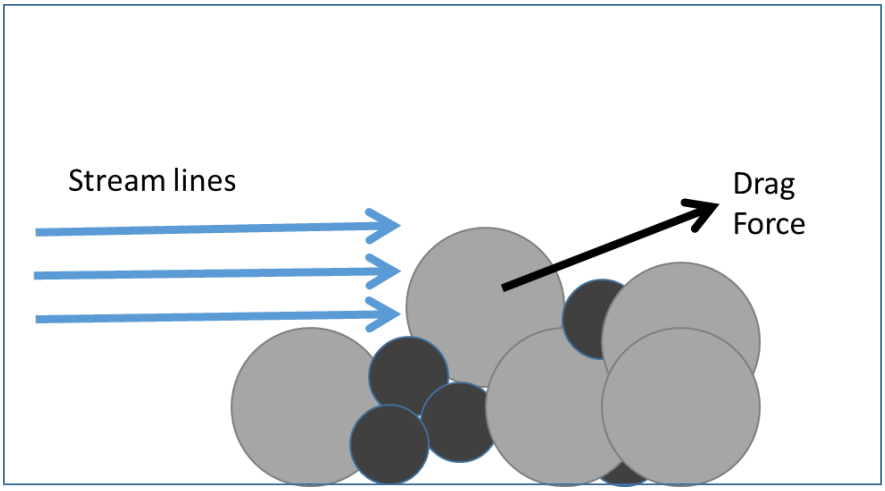

Figure 42: Sketch of t the 1 mm particles located among the 2 mm particles and protected from the flow.

Figure 42 can be understood as the 2 mm particles protect the small particles from the hydrodynamic forces (drag force) generated by the stream-wise. For this reason, few seconds after starting the run the 2 mm particles are observed to accumulate close to the inner wall first than the small particles, see Figure 41-b.

After the 1 mm particles are no longer protected for the 2 mm particles, many of them start to roll at the same time; being dragged towards the inner wall with a more inclined direction comparing with the 2 mm particles. The majority of them move easily upward to the top parts of the bed, the path that they follow varies a lot because it depends on the "obstacles that they can meet" like for example if they meet big particles in its way they can stop or change its direction even more titled up. The velocity of the 1 mm particle climbing to the bed top is higher than the 2 mm particles moving around the bed border. The reason of this is that the liquid velocity increases rapidly near the channel bottom until few millimeters (10 mm) above this, so when the 1 mm particles start to climb, they are dragged with a higher fluid force than the fluid force acting over the 2 mm particle in contact with the bottom channel; see figure below. Furthermore, 1 mm particles are lighter so the flow can transport them through longer much easier.

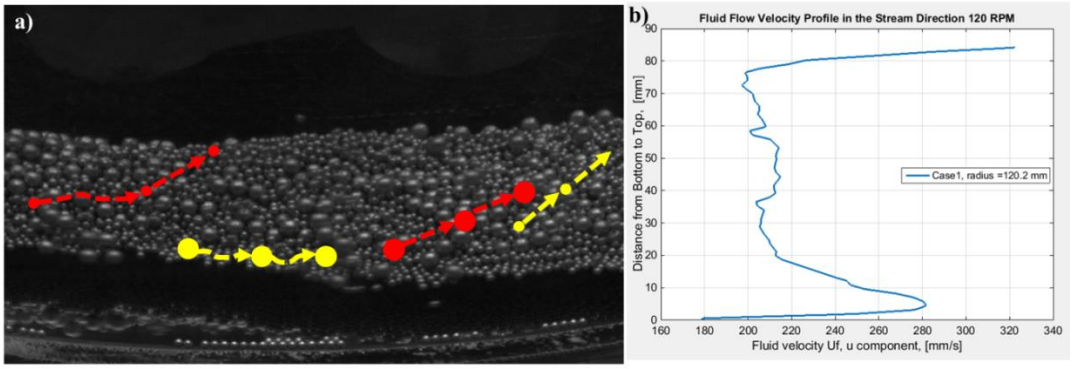

Figure 43: 1 mm and 2 mm particles motion during the transition period. Lid rotation speed 120RPM. Particle motion was tracked visually/manually as explained earlier in the text.

As we can see in the graph above there is a mix of 1 mm and 2 mm particles during the transition period but once the fully developed state is achieved mostly the 1 mm particles are around the inner wall and the 2 mm are around the 1 mm particles, so the question is how a separation takes place? To find the answer to this important question was necessary to run the experiment twice without blinking.

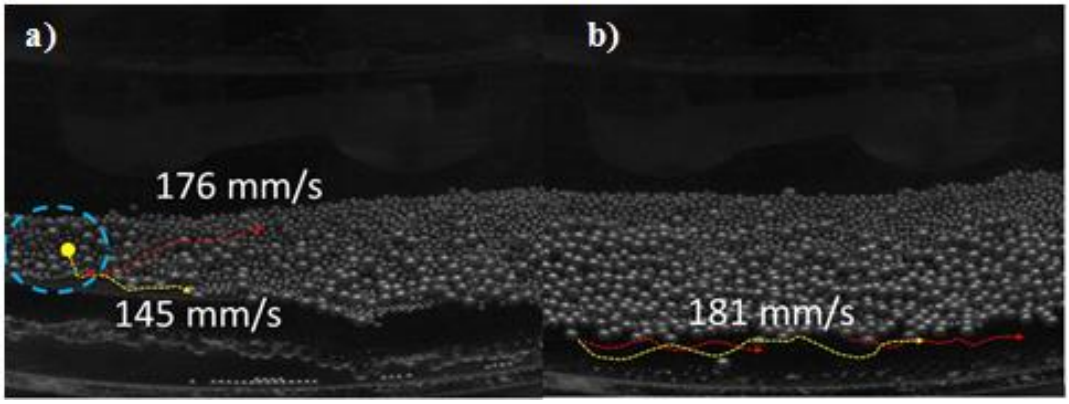

Figure 44: a) 1 mm particle & 2 mm particles separation, b) bed geometry at fully developed flow at 120 RPM. Visual / manual particle tracking as explained earlier in the text.

At Figure 44-a) it is interesting to notice that before there were more particles of 2 mm at the top of the bed close to the inner wall and now almost only the 1 mm particles are visible. Of course, some 2 mm particle could be buried by the smallest ones since these are easier dragged to the top of the bed. But please see the blue dashed circle. Here erosion process is taken place, we should not expect that the big particles will fall down but there is an interesting situation:

First, the packing system of the bed is not a stable one. This can be seen as the hillside of a dune; where in this case the big particles are protecting the small ones from the fluid stream and the small particles are like the base of this structure. Then if the base is eroded the whole structure will fall down. What happens is the following: first, layer of the bed is being eroded by the flow or for the impact of the particles coming in the moving layer (around the bed border), so as the bed is eroded the

particles slide down and two situations now occur: 1) the big particles (2 mm) will be dragged and transport in the moving layer; this means around the bed border and 2) the 1 mm particles will be transported for a short period inside the moving layer until they are lifted and dragged again to top of the bed or a higher position in the bed (red dashed line represents the 1 mm particle path and the yellow lines represents the 2 mm particle path after sliding down the hillside). The Saffman lift force is responsible of removing very fast the small particles (1 mm) from the moving layer, a differential pressure is created between the top and bottom of the particle due to the velocity gradient lifting the particle very short vertical distance and then the secondary flow drags it. Off course for the 2 mm particle also there is present a differential pressure but it is not large enough to overcome the submerged weight of the 2 mm particle.

Based on the previous observation, we explain how the particles are separated so when the fully developed state is achieved the 1 mm particles are mostly around the inner wall and the 2 mm are mostly around the 1 mm as mentioned before.

At Figure 44-b) the obtained bed at the fully developed state is shown. At this moment mainly the particles of diameter equal to 2 mm moved by rolling around the border of the obtained bed. In the figure, the red and yellow lines indicate the typical particles motion. In order to appreciate easier where particles move at fully developed state, two consecutive pictures are subtracted using Matlab. The end result is the Figure 45-c) where the white marks represent what has changed from picture 1 to picture 2 that is the particles that are moving, in other words, the movement zone.

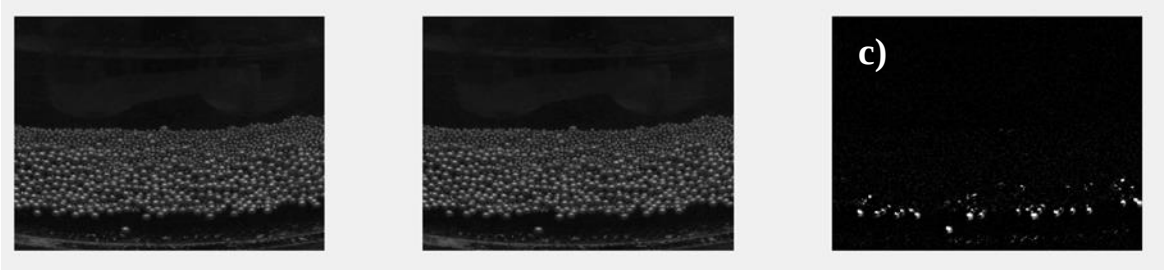

Figure 45: Motion of mixture of particles at developed state. From left to right; Picture at time t, picture at time t+1 and particles motion region, respectively.

4.6) Particle concentration vs bed geometry

The aim of this section is to study how the bed geometry changes when the particle concertation is increased. The reference point is one of the previously described experiment; the mixture of particles of 1 mm and 2 mm diameter with 100 grams in total of each particle size at 120 rpm. For the new run the weight of particles was doubled to 200 grams in total of 1 mm particle diameter and 200 grams in total of 2 mm particle diameter keeping the other parameters unchanged (120 rpm, manually distributed bed; deionized water and so on). Furthermore, the lid spindle speed was increased to see how this affects the bed morphology.

Table 6: Test matrix for particle concentration vs bed geometry

Experimental Run	Lid rotation	Fluid	Bed	Particles size	Particle concentration
1-LPC (Low particle concentration)	120 RPM	Deionized water	Manually organized plane bed	Mixture of 1 mm and 2 mm particle diameter	In total 200 grams
2- HPC (High particle concentration)					In total 400 grams

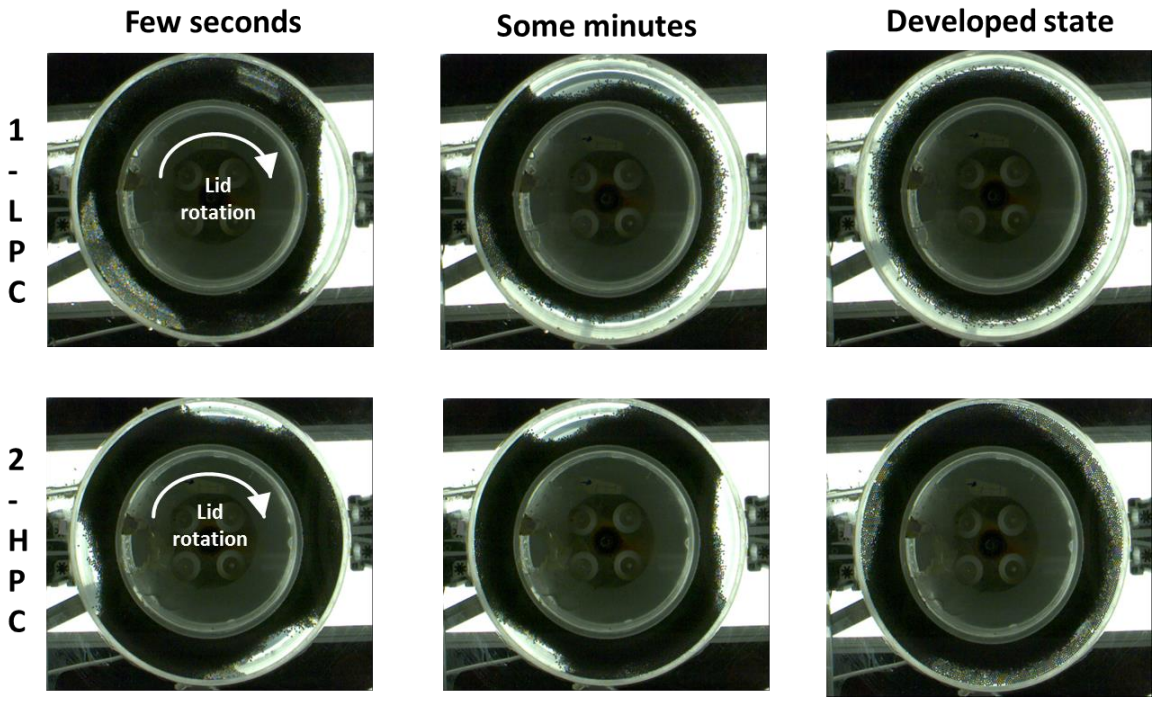

Figure 46: Bed geometry at different particle concentration for the mixture of particles at 120 rpm. Lid rotation: clockwise.

Figure 46 displays the bed geometry changes with the time for the two cases, the 200 grams (first row) and 400 grams (second row) of a mixture of particles. Few seconds after starting the experiments the first differences are observed:

- For the high particle concentration, three fans are developed and they remain almost during all the run. While for the low particle concentration; 2 fans can be seen and after some minutes only 1 remains.
- The obtained fans are not static, they slowly change position. How? Particles are eroded at the front of one of the fan and move toward the tail of the next fan in the main flow direction. Some of these particles climb and others just stop and accumulate at the tail so in this order the fans appear to change position.

- For the LPC case at the fully developed state, no more fans are presented; all particles are now forming a ring around the inner wall. Mainly the big particles are rolling around the bed border at the bottom. While for the HPC case there are 2 fans.

- For the HPC case, between the fans first there was an empty space, here called "particle free space". However, with the time more 2 mm particles are separated from the 1 mm particles (close inner wall) and transported around the bed perimeter (see the red dotted line figure below). As a result, they tend to fill those empty spaces between the fans creating a monolayer of 2 mm particles. The separation phenomenon is the same as described before.

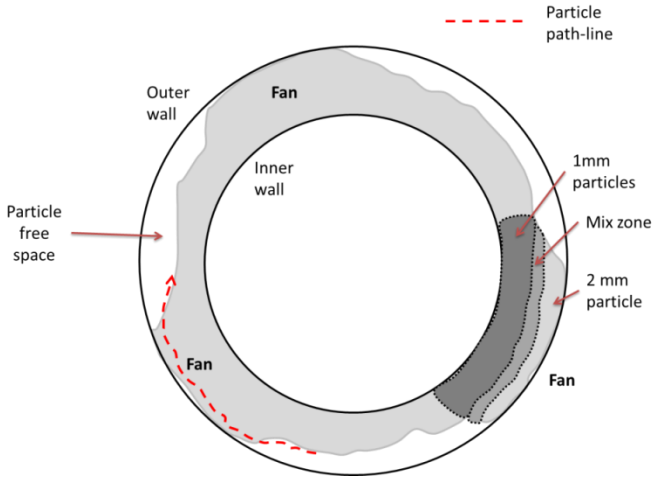

Figure 47: Arrangement of particles within a fan for the mixture of 2 mm and 1 mm particle diameter. Visual tracking as described.

On the other hand, from a closer inspection during the developed state it is seen that particles at the fans are deposited or located in the following way: 1 mm particles adjacent to the inner wall, a mixing zone around the 1 mm particles and finally the 2 mm particles in the remaining space (in contact with the outer wall), see figure above. The particles that move over the fans are mostly the 2 mm particle diameter, they move by rolling around and over the mixing zone and over 2 mm particles zone; the movement is parallel to the main flow direction. This does not mean that the 1 mm particles are totally static but their movements are very sporadic over short distances and principally diagonal toward the inner wall.

After the developed state was achieved, the lid's spindle speed was increased to 160 rpm generating four fans. Then at 200 rpm still the same numbers of fans are observed but they are changing position very fast until one of the fans disappears (remaining only 3). After few minutes the shape of these fans is less noticeable (well defined). Finally, at 220 rpm the fans totally disappear and very dense flow regime of the 2 mm particles is generated, much less 1 mm particles moved by rolling close to the inner wall.

From this analysis, at developed state, it is clear that a low particle concentration (initial thin bed) self-organized fan forms are not present. Instead a ring around the inner wall is the final bed form. However, when increasing the particle concentration (thick bed) to a high enough value some fans will remain and they slowly change position. Moreover, when increasing the lid rotation even more fans are developed up to certain rotational speed where they are removed. It is believed by the author based on the visual observation that if the present experiment for the thick bed (high particle concentration) is done by taking into account the long-term evolution, that is to run the experiment for some days, it will be found that the amount of particles that are eroded from a fan is the same as the number of particles that are deposited. In other words, a saturated surface density of moving particles will be obtained. This will be in agreement with (Charru et al., 2004).

But lets us try to understand why the fans obtained for the thick bed are present even at the developed state. It is very important to notice first that the velocity of the lid is the same for the thin and thick bed. This gives us the idea that the hydrodynamic forces may not change abruptly since it is the lid which drags the fluid and the fluid drags the particles. First, it was observed that the maximum high of the bed (adjacent to the inner wall) after the runs varies little for both cases. But here we also must understand that the particle concentration was doubled then that small variation in height can be neglected if compared with the number of particles that were added. So with this, we want to say that the fluid forces are no able to pull particles to a much higher level, and since the double of particles are present for the thick bed, those particles have to be also deposited somewhere. As a result, they form the fans. To conclude, if an adequate lid spindle speed is used (120 rpm for instance) then self-organized fan geometries are obtained, slightly dependent on the total particle volume. There should be a certain particle concentration or particle volume for below which no fans are generated.

This experiment was also repeated for the single 2 mm size particles; particles were doubled to 200 grams. This means that the first run was for 100 grams and the second for the double. How the bed is eroded is the same as explained before but occurring mostly int the uppermost layers. However in this occasion, the first layer of the bed was never eroded (time of experiment > 2 hours) and no fan(s) was generated. In the beginning, the height of the bed was 2 particle diameters and there were few particles above this. Then as a result particles in the second layer of the plane bed and above this were dragged inwards, thus forming a ring of particles around the inner wall. At the end, only some particles moved around the border of this ring by rolling over the particles in the first layer and in contact with the particles in the border. Since no fans were observed at the end of the run and in order to verify the hypothesis that this kind of geometry depends on the amount of particles, it was decided to increase again the particle concentration to 400 grams. This run shows two things: 1) the first and second layers of particles were never eroded and 2) no fans were created, pictures of this are presented in the power point file. As a result, we concluded that it is not always true that the formation of bed fans occurs for

all possible high particle concentration. On the contrary, it also depends on the particle size(s). This new outcome led to a new experiment:

The experiment consists of: a mixture of particles of 1 mm, 2 mm and 0.5 mm particle diameter, deionized water and lid rotation speed of 120RPM. First 100 grams of each particle size was used and afterwards another 100 grams extra of 0.5 mm particles size were added. The following are the most relevant outcomes:

- For the first case (100 grams of each particle size, 300 gr in total) no bed fans were clearly created.
- For the second case (100 grams of 1 mm and 2 mm particles and 200 grams of 0.5 mm particles, 400 gr in total) 3 fans are obtained. In this case also when increasing the angular speed the number of fans increases and if this rotation speed is large the fans disappear.

To close this section, the generation of fans as bed form depends directly on the particle concentration or amount of particles and the particle size. For relatively large and heavy particles (Ø 2 mm) no fans are created. On the contrary, for small particles we obtain fans as bed geometry; the number of fans tends to increase with the lid rotation speed until the point where they vanish.

4.7) Morphology and displacement of dunes in a cylindrical cell

The objective here is to understand some features of the dynamics of isolated dunes in a cylindrical cell, notably the deformation and if the particles could be transported as single dune under low rpm (120 rpm). For this experiment the spherical particles of aluminum of mean diameter equal to 2 mm, 1 mm and 0.5 mm were used; first one dune and two dunes of single size particles of 2 mm were created and after two dunes formed by a mixture of particles of the 3 different sizes spheres were analyzed. Pictures for the 2 mm particles diameter were recorded and are presented here. Moreover, pictures of the mixture of particles are in the PowerPoint file "Isolated Dune-Particles Transportation". In short, the following three cases were studied:

Table 7: Test matrix for displacement of dunes in a cylindrical cell

Case	Dunes	Particles-Weight (in total per case)	Particles mean diameter	Lid rotation speed (RPM)
1	One	50 grams in total	2 mm	120
2	Two	100 grams in total		
3	Two	No recorded	2 mm, 1 mm & 0.5 mm	120

The experimental procedure for each was as follows: the single(s) dune(s) was built up by dumping the weighted particles, contained in a cylindrical container; from above of the annular channel and with a spoon the particles that went far from the dune were moved towards this. The annular channel was already filled with deionized water. Then the lid was put in place and fixed to the spindle. Then, the LED illumination panel was put over the annular setup and the bottom and side view cameras were calibrated. After everything was in place, the lid rotation speed was set constant to 120 rpm.

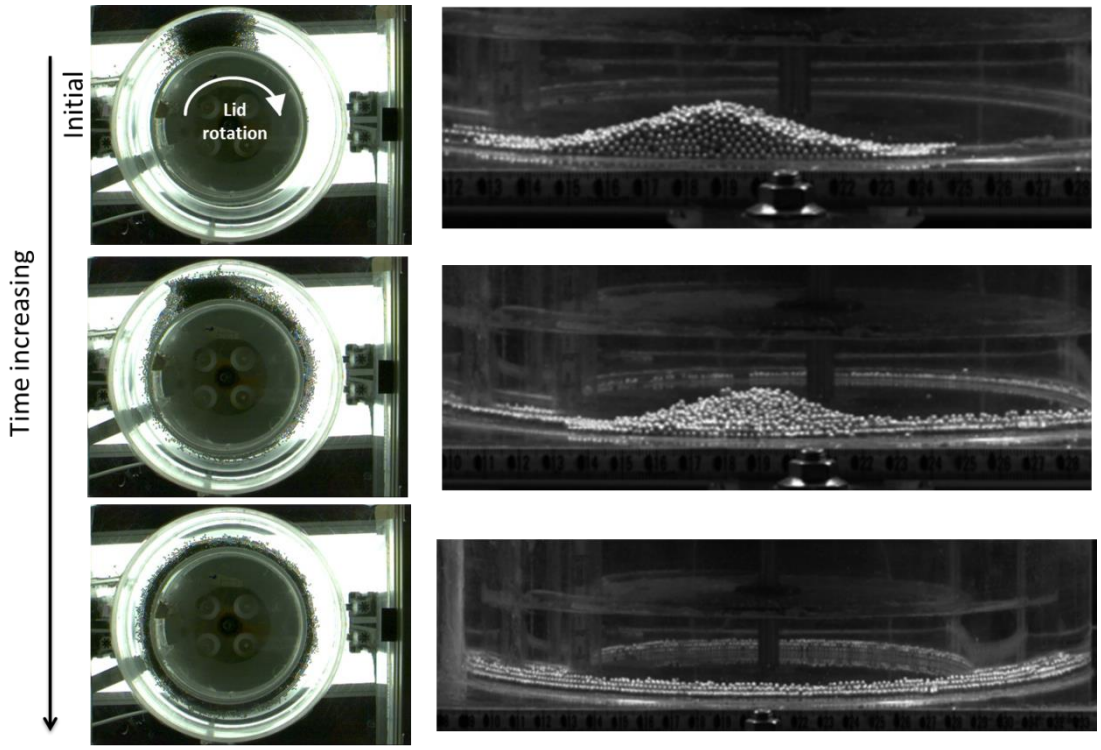

Figure 48: Transport of a single dune; single size particle diameter; 2 mm at 120 rpm. Lid rotation: clockwise and for the side view pictures from left to right.

For the two first cases as the upper plate attains the desired rotation speed, primary the particles in the border front of the dune are swept towards the rotation center by rolling in permanent contact with the dune front. This motion reflects the pure effect of the secondary flow since as it was observed by (Franklin & Charru, 2009) and it is well-known particles in the front of a dune are not entrained in the main direction of the flow due to the recirculation zone created downstream from the dune crest. As particles in the border front are being removed this causes a destabilization of the front of the dune generating small avalanches. Particles that fall within the avalanches move towards the inner wall. Then after few seconds erosion starts to take place at the region called “upwind side” (see Figure 49) where particles are eroded and transported to the dune crest and dune front. This erosion occurs first for half of the dune; particles located between the outer wall and the middle of the annular channel were first eroded and dragged. This situation is explained by the fluid flow velocity profile, see the

figure in Appendix A (3D flow velocity profile for 120PM) where it is clearly seen that the liquid velocity is larger in that region so particles can be easier entrained and transported. Then the remaining part of the dune is a slower pace deformed and a ring of particles around the inner wall is observed.

On the other hand, when the dune is made up of big particles (Ø=2 mm & Ø=1 mm) and small particles (Ø=0.5 mm) is more difficult to remove it. In other words, it takes much more time to deformer the dune; dragging the particle around the channel, because the recirculation flow created at the front of this type of bed geometry causes to some small particles (0.5 mm) to return to the surface of the front of the dune, see Figure 49. While with the large particles it is not capable and these are dredged towards the inner wall. Then the dune is preserved for a longer time. However, in both cases, single size and a mixture of particles, the dune(s) are destroyed and particles moved and accumulated around the inner wall.

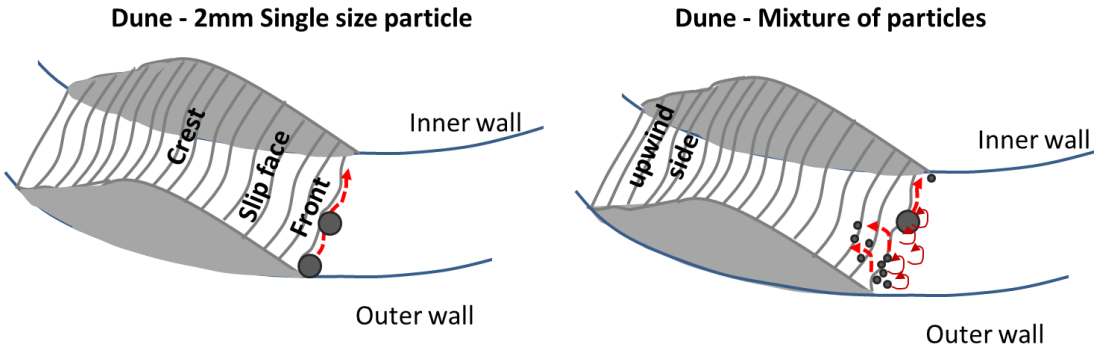

Figure 49: Sketch of single dune particles transportation. Lid rotation: clockwise.

For a cylindrical cell where the secondary flow is presented in such a way that it cannot be neglected or neutralized, particles could not move as a single dune because of the nature of the liquid velocity profile as mentioned before. In other words, the lack of a uniform liquid velocity in the annular channel therefore will make single dune transport impossible. This velocity profile causes the particles in the border front of the dune to move towards the inner wall first and then part (half or one quarter) of the dune width is removed. Finally, the section or particles in the dune adjacent to the inner wall are swept and the dune disappears.

4.8) Extra observations

It was observed that after stopping the experiments, setting the lid rotation speed zero, for some hours and then starting it again; particles that earlier were moving, now didn't immediately move. They remained motionless even one hour after the flow was restarted under the same conditions that it

was before. This agrees with (Charru et al., 2004) who appreciated the same situation concluding that the threshold for particle motion is higher and explained this situation as consequences of the rearrangement of the surface microstructure. However, it is important to notice that in their case the secondary flow was insignificant. In our case is not still clear what the driver of this is.

It was also seen that the time at which the manually created bed starts to be eroded varies with the way in which the experiment is run, that is how the lid rotation speed is set. For some experiments, the revolutions per minute of the upper plate were increased periodically in steps of 20 rpm starting from zero. Once the speed of the lid achieved 120 rpm it took to the flow around 7 to 8 minutes (for the 2 mm bed-particles) to begin eroding the thin-bed (first layer) while if the upper plates velocity was set immediately at 120 rpm after the bed was created; the flow only needed few seconds to drag the particles within the bed. It is believed, as it was mentioned, that the secondary flow acts as another "gravitational force" but in radial direction (centripetal/centrifugal) compacting the bed-particles. Then if the bed-particles are exposed to the action of this force for longer time, even at low RPM when the hydrodynamic forces are not able to entrain the particles that is the case when increasing the RPMs step by step, the bed-particles are placed closer among them what may give rise to the Van der Waal's force and this makes more difficult to move each particle. Furthermore, as the particles are closer to each other, they protect themselves against the fluid forces. This situation can be interpreted as a rise of the threshold Shields numbers that corresponds to an 'armoring' of the bed what it is mentioned by (Charru et al., 2004) but in our case as a consequence of the action of the secondary flow.

The motion track and speed of the aluminum particles for three specific cases; single size particle 2 mm, mixture of particles of 1 mm and 2 mm and single size particles of 1 mm median diameter are reported in the annexed PowerPoint filed called "Particles motion and speed at 120 RPM. These results and the discussion are not shown here, to avoid including too many pictures.

Also, flattened particles were made out from the 2 mm aluminum spherical particles using the tools and equipment display in Figure C - 7. The intention with this was to study the dynamics of these new shape particles and run them together with the spherical particles, but due to the lack of extra time and the detailed work that this demands, this work is addressed as a recommendation for a future investigation.

Finally, further investigations that need to be carried out include: use a Non-Newtonian fluid (PAC- polyanionic cellulose for instance), use different particle shape (flat particles or irregular shape particles) and another recommendation is to rebuild the lid in such a way that it is possible to see through this and a high-speed video camera can be place pointed from above.

Chapter 5

5) Conclusion

Many experiments regarding the liquid-particle interaction (particle dynamics) like the cuttings transport in petroleum drilling operations and transport of sediments in rivers have been conducted at laboratories. In both cases either pipes or flumes were commonly used; however, for both situations, a constant particle feeding is problematic when it is necessary. With the present set-up, cylindrical cell, this is avoided and mass conservation is ensured. There are very few reported cases where this has been utilized. Furthermore, in those cases, the upper plate rotation speed was controlled and the relative measurement among the fluid height, the annular width, the bed thickness was designed in such a way that the secondary flow was very weak and therefore neglected. The author of this project report described some relevant features of the dynamics of particles and the liquid flow profile (with the presence of the secondary flow) in a continuous circular annular channel. It was done by means of experimental observations in order to provide a background for further investigations taking into account the limited literature available. For instance, the created secondary flow in the current flow is similar as the effect of the rotating drill string in the wellbore in a horizontal section. It is possible to study in more detail how cuttings are piled up against the borehole by the action of the rotation of the drill string.

From the PIV analysis, it was showed that the azimuthal liquid velocity does not decrease linearly from the lid velocity at the upper plate to zero at the bottom (Plane to Couette flow). In this case, the liquid velocity at bottom wall must be zero, and at the lid must be the angular velocity because of the non-slip condition. However, a rapid increase of the liquid velocity near the bottom wall is observed due to the action of a secondary flow that goes inwards at the bottom of the channel. Subsequently, the liquid velocity diminishes to a relatively constant speed and finally, there is a steeply increment very close the lid.

The transportation mode of the three main size of particles of median diameter equal to 2 mm, 1 mm and 0.5 mm was studied at 120 rpm and 140 rpm. At these upper plate speeds, the 1 mm and 2 mm particles were transported mainly by rolling/sliding and the 0.5 mm particles were moving by small jumps, (similar to saltating flow regime). Also, some of these small particles were affected by the turbulence and, consequently, those particles moved into suspension.

Larger single size particles (2 mm) tend to form a well-defined packing system with layers around the inner wall. At developed state, this kind of packing at the border (bed-border) is more difficult to erode; so particles in the border remain stable until other particles impact them. Furthermore, once the 2 mm particles are transported and deposited adjacent to the inner cylinder wall the hydrodynamic forces are not able to entrain and transport them again. Meanwhile, a mixture of particles (small and

big particles) forms an unstable ring bed form around the inner wall. In this case, when the bed border is eroded then small avalanches occur falling down all the particles on the ring bed surface. This phenomenon gives rise to the separation of the 1 mm and 2 mm size particles since once the 2 mm particles fall down to the bottom of the bed, the flow is only capable of transport these around the bed border. On the contrary, once the 1 mm particles fall down the hydrodynamic forces are capable to transport them again to the bed surface and to higher levels. As a result, when the fully developed state is achieved, the smaller size particles are mostly found around the inner wall and the big size particles are mainly found around them.

It was observed experimentally two different types of bed form at fully developed state; a continuous ring around the inner wall and self-organized fans. The generation of self-organized fans depends on the particle concentration or amount of particles and the particle size. For relative large and heavy particles (2 mm) no fans are created. Instead, when the 2 mm particle concentration is increased the deepest bed layer(s) are not eroded. On the contrary, for small particles we obtain fans as bed geometry; the number of fans tends to increase with the lid rotation speed until the point where they vanish.

(Franklin & Charru, 2009) investigated the displacement and deformation of isolated dunes by a water flow in a horizontal closed conduit. They observed that an initial pile of beads, of different sizes, is rapidly deformed by the flow, adopting a “croissant” shape, like barchan dunes and this dune moved maintaining this form. It was found experimentally that the motion of isolated dunes in a circular annular channel is not possible due to the lack of a uniform liquid velocity across the channel. Moreover, we observed that the deformation of a dune formed by 2 mm size particles occurs faster than for a dune composed of a mixture of particles (d=1 mm, 2 mm & 0,5 mm). The final bed morphology is the form of a ring around the inner wall.

References

Bagnold, R. (1956). The Flow of Cohesionless Grains in Fluids Phil. Trans. R. Soc. Lond. A December 18, 1956 249: 235-297; doi: 10.1098/rsta. 1956.0020.

Bagnold, R. A. (1954). Experiments on a gravity-free dispersion of large solid spheres in a Newtonian fluid under shear. *Proceedings of the Royal Society of London. Series A. Mathematical and Physical Sciences, 225*(1160), 49-63.

Bagnold, R. A. (1956). The flow of cohesionless grains in fluids. *Phil. Trans. R. Soc. Lond. Series A, Mathematical and Physical Sciences, 249*(964), 235-297. doi:10.1098/rsta.1956.0020

Bagnold, R. A. (1973). The nature of saltation and of 'bed-load' transport in water. *Proc. Roy. Soc. London, Series A., 332*(1591).

Ben Crosby, a. K. W. (Fall 2006). *12.163 Surface Processes and Landscape Evolution. Massachusetts Institute of Technology: MIT OpenCourseWare,*. In. Retrieved from https://ocw.mit.edu. License: Creative Commons BY-NC-SA

Betat, A., Frette, V., & Rehberg, I. (1999). Sand ripples induced by water shear flow in an annular channel. *Physical Review Letters, 83*(1), 88-91. doi:10.1103/PhysRevLett.83.88

Charru, F., Bouteloup, J., Bonometti, T., & Lacaze, L. (2016). Sediment transport and bedforms: a numerical study of two-phase viscous shear flow. *Meccanica, 51*(12), 3055-3065. doi:10.1007/s11012-016-0553-5

Charru, F., Mouilleron, H., & Eiff, O. (2004). Erosion and deposition of particles on a bed sheared by a viscous flow. *Journal of Fluid Mechanics, 519*, 55-80. doi:10.1017/S0022112004001028

Clift, R., Grace, J. R., & Weber, M. E. (2005). *Bubbles, drops, and particles*: Courier Corporation.

Cocks, D. (2005). *Mathematical modelling of dune formation.* (Doctor of Philoophy), University of Oxford,

Dey, S., & Ali, S. Z. (2017). Mechanics of sediment transport: Particle scale of entrainment to continuum scale of bedload flux. *Journal of Engineering Mechanics, 143*(11). doi:10.1061/(ASCE)EM.1943-7889.0001343

Einstein, H. A. (1950). *The bed-load function for sediment transportation in open channel flows* (Vol. 1026): Citeseer.

Fernandez Luque, R. (1974). Erosion And Transport Of Bed-Load Sediment.

Fernandez Luque, R., & Van Beek, R. (1976). Erosion And Transport Of Bed-Load Sediment. *Journal of Hydraulic Research, 14*(2), 127-144. doi:10.1080/00221687609499677

Fluid Mechanics D203. In D.J.DUNN (Ed.), *Tutorial No. 1, Fuid FLow Theory*. Retrieved from https://edoc.site/fluid-mechanics-d203-pdf-free.html

Francis, J. R. D. (1973). Experiments on the motion of solitary grains along the bed of a water-stream. *PROC. ROY. SOC. LONDON, SERIES A*(332 , no.1591 (1973)), 443-471.

Franklin, E. M., & Charru, F. (2009). Morphology and displacement of dunes in a closed-conduit flow. *Powder Technology, 190*(1-2), 247-251. doi:10.1016/j.powtec.2008.04.065

John Southard. (Fall 2006). *12.090 Introduction to Fluid Motions, Sediment Transport, and Current-Generated Sedimentary Structures. Massachusetts Institute of Technology: MIT OpenCourseWare*. In. Retrieved from https://ocw.mit.edu. License: Creative Commons BY-NC-SA

Johnsen, M. S. (2014). Particle transport and hole cleaning in wells during drilling. In: University of Stavanger, Norway.

Khatibi, M., Time, R. W., & Rabenjafimanantsoa, H. A. (2016). Particles falling through viscoelastic non-Newtonian flows in a horizontal rectangular channel analyzed with PIV and PTV techniques. *Journal of Non-Newtonian Fluid Mechanics, 235*, 143-153. doi:10.1016/j.jnnfm.2016.08.004

Lajeunesse, E., Malverti, L., & Charru, F. (2010). Bed load transport in turbulent flow at the grain scale: Experiments and modeling. *Journal of Geophysical Research: Earth Surface, 115*(4). doi:10.1029/2009JF001628

Meyer-Peter, E., & Müller, R. (1948). *Formulas for bed-load transport.* Paper presented at the IAHSR 2nd meeting, Stockholm, appendix 2.

Rheosense. Viscosity of Newtonian and non-Newtonian Fluids. Retrieved from http://www.rheosense.com/applications/viscosity/newtonian-non-newtonian

Schwarzkopf, J. D., Sommerfeld, M., Crowe, C. T., & Tsuji, Y. (2011). *Multiphase flows with droplets and particles*: CRC press.

Secondary flow. (2011). Retrieved from http://www.thermopedia.com/content/1113

Thielicke, W., & Stamhuis, E. (2014). PIVlab–towards user-friendly, affordable and accurate digital particle image velocimetry in MATLAB. *Journal of Open Research Software, 2*(1).

Westerweel, J. (1997). Fundamentals of digital particle image velocimetry. *Measurement science and technology, 8*(12), 1379.

Appendices

Appendix A

A. 3D fluid flow velocity profile plots

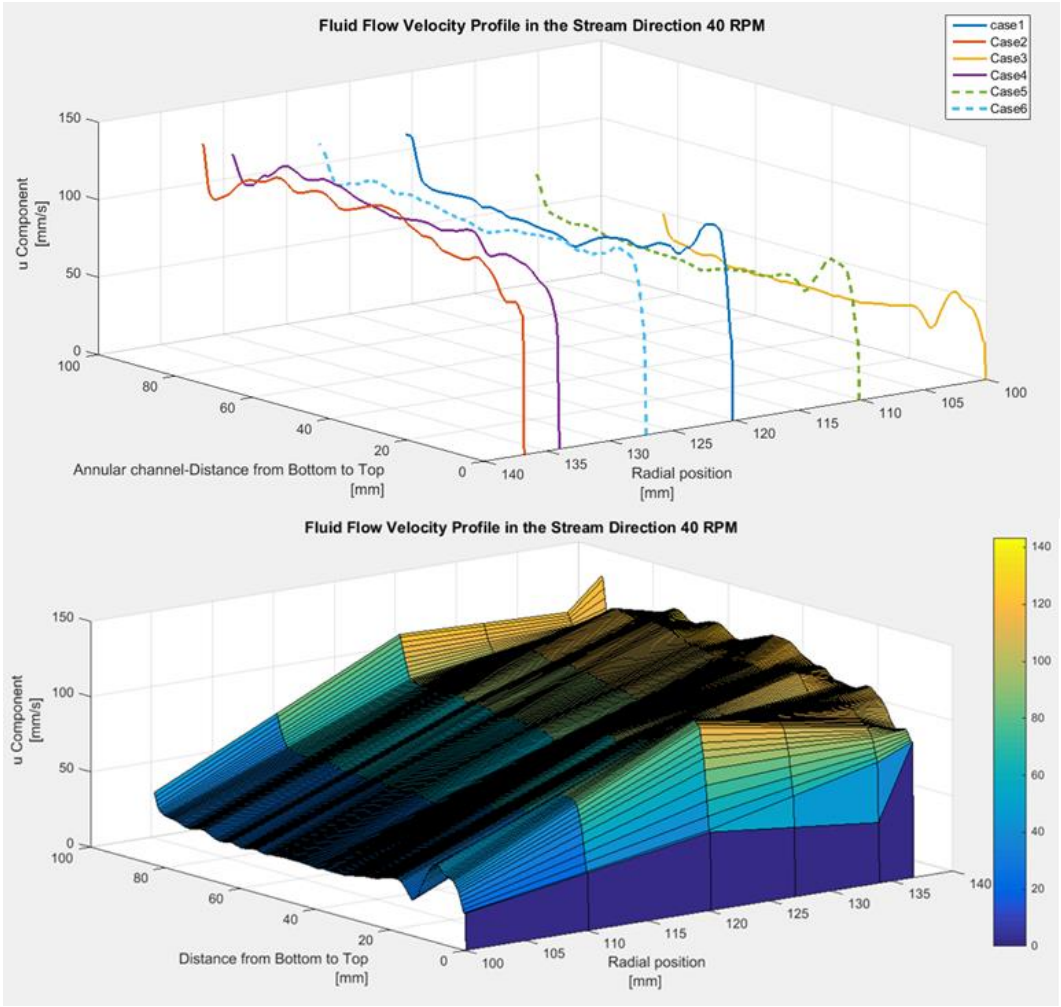

Figure A - 1: 3D Liquid velocity profile in the annular channel at 40 rpm

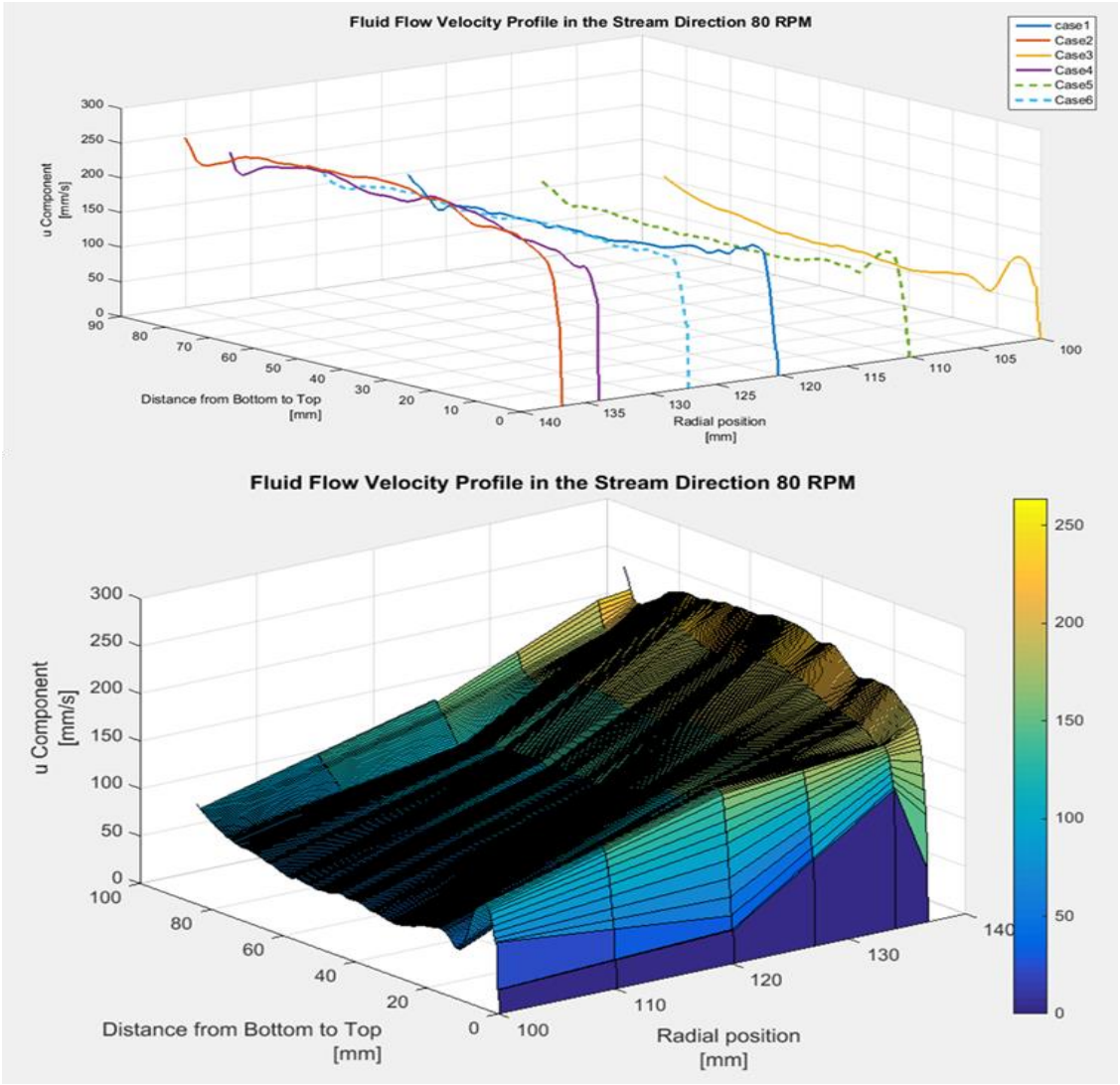

Figure A - 2: 3D Liquid velocity profile in the annular channel at 80 rpm

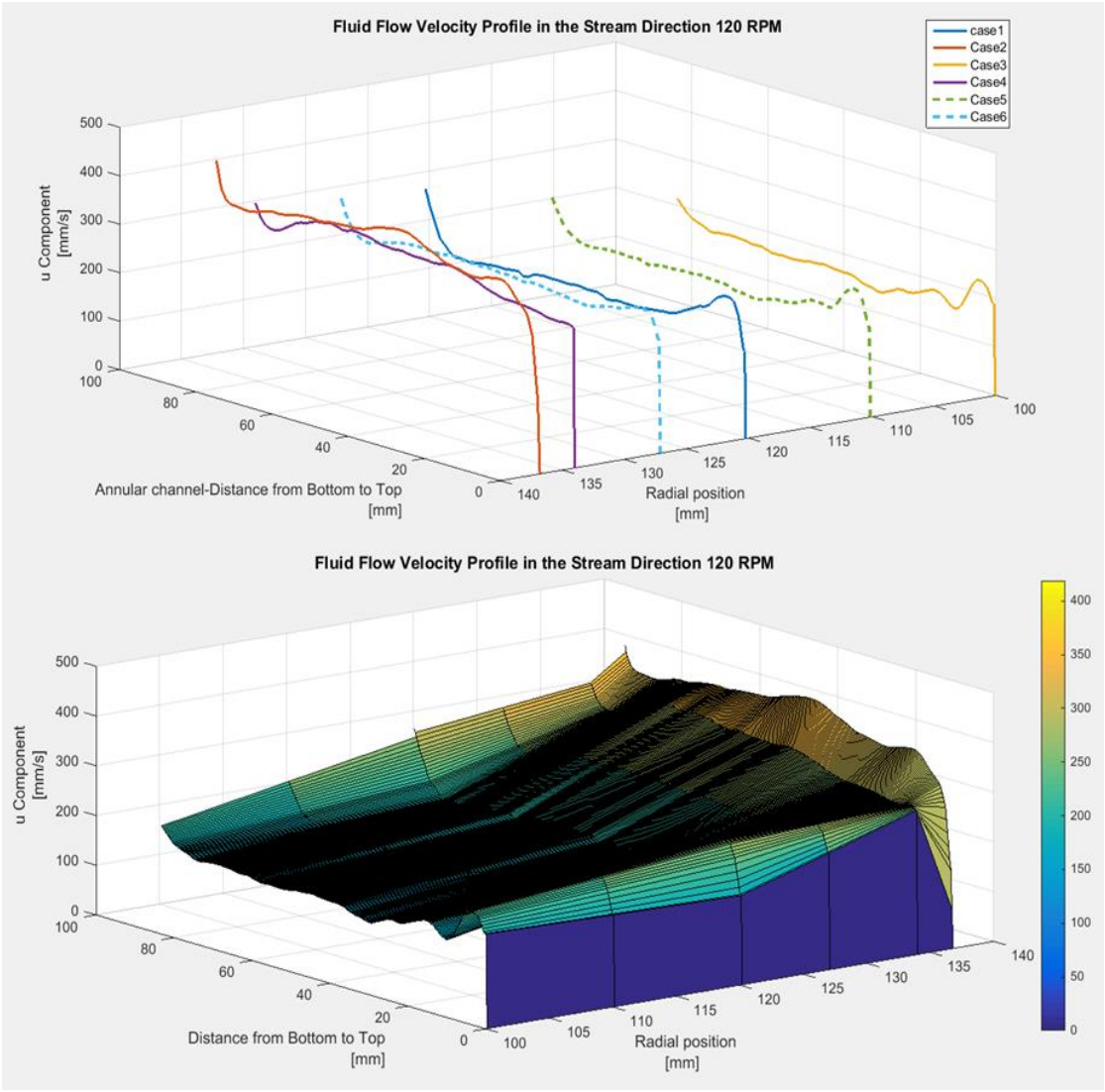

Figure A - 3: 3D Liquid velocity profile in the annular channel at 20 rpm

Appendix B

B. Matlab Script for the 3D flow velocity profile plots

```
close all,clear all, clc

%The number of velocity points that were exported from PIVlab is 300 then
%the .txt files have 2 columns and 301 rows (first row is the headers)

%Import data from text file
filename = 'u_component_case1_2000rpm_1.txt';
filename_2='u_component_case2_2000rpm_1.txt';
filename_3='u_component_case3_2000rpm_2.txt';
filename_4='u_component_case4_2000rpm_1.txt';

delimiter = ','; %type of delimiter
startRow = 2; % Import data starting from the second row

formatSpec = '%f%f%[^\n\r]'; %format string

fileID = fopen(filename,'r');  %Open the text file
fileID_2=fopen(filename_2,'r');
fileID_3=fopen(filename_3,'r');
fileID_4=fopen(filename_4,'r');


% Read columns of data according to format string.
dataArray = textscan(fileID, formatSpec, 'Delimiter', delimiter,
'MultipleDelimsAsOne', true, 'EmptyValue' ,0.0,'HeaderLines' ,startRow-1,
'ReturnOnError', false);
dataArray_2 = textscan(fileID_2, formatSpec, 'Delimiter', delimiter,
'MultipleDelimsAsOne', true, 'EmptyValue' ,0.0,'HeaderLines' ,startRow-1,
'ReturnOnError', false);
dataArray_3 = textscan(fileID_3, formatSpec, 'Delimiter', delimiter,
'MultipleDelimsAsOne', true, 'EmptyValue' ,0.0,'HeaderLines' ,startRow-1,
'ReturnOnError', false);
dataArray_4 = textscan(fileID_4, formatSpec, 'Delimiter', delimiter,
'MultipleDelimsAsOne', true, 'EmptyValue' ,0.0,'HeaderLines' ,startRow-1,
'ReturnOnError', false);

fclose(fileID);
fclose(fileID_2);
fclose(fileID_3);
fclose(fileID_4);

%Allocate imported array to column vectors
d_case1 =1000*dataArray{:, 1}; % distance [mm], 1000 is to convert from m
u_case1 = 1000*dataArray{:, 2}; % to mm
d_case2 = 1000*dataArray_2{:, 1};
u_case2 = 1000*dataArray_2{:, 2};% velocity [mm/s]
d_case3 = 1000*dataArray_3{:, 1};
u_case3 = 1000*dataArray_3{:, 2};
d_case4 = 1000*dataArray_4{:, 1};
u_case4 = 1000*dataArray_4{:, 2};

%establish position/radius where the light sheet was shot for each case
r1=120.2;
r2=136.8;
```

```
r3=100.1;
r4=134.0;
[n] = length (u_case1);

%Create a vector of 1xn radius value
r_case1=linspace(r1,r1,n); % radius at laser position 1
r_case2=linspace(r2,r2,n); % radius at laser position 2
r_case3=linspace(r3,r3,n); % radius at laser position 3
r_case4=linspace(r4,r4,n); % radius at laser position 4

L=85; %length from the bottom to the top of the channel
s=L/(n-1);
d=(0:s:L)';

%In order to get the surface plot it is necessary to have a matrix (M)
%where the first column is the distance from 0 to 85 and the remaining
%columns are the velocity at each radius

%linear interpolation to obtain velocity values for the same distance steps
%for all velocity vectors
u_i_case1 =interp1(d_case1,u_case1,d);
u_i_case2 =interp1(d_case2,u_case2,d);
u_i_case3 =interp1(d_case3,u_case3,d);
u_i_case4 =interp1(d_case4,u_case4,d);

% generating matrix M
M(:,1)=d;
M(:,2)=u_i_case1;
M(:,3)=u_i_case2;
M(:,4)=u_i_case3;
M(:,5)=u_i_case4;

M(1,:)=0; %the velocity value at bottom must be zero

%In some cases the values of velocity close to the bottom are NaN (non a
%number) along the curve for a given radius so here those values are
%generated by interpolation
M(2,3)=((d(3)-d(2))/(d(3)-d(1)))*M(1,3)+((d(2)-d(1))/(d(3)-d(1)))*M(3,3);
M(2,4)=((d(4)-d(2))/(d(4)-d(1)))*M(1,4)+((d(2)-d(1))/(d(4)-d(1)))*M(4,4);
M(3,4)=((d(4)-d(2))/(d(4)-d(1)))*M(1,4)+((d(2)-d(1))/(d(4)-d(1)))*M(4,4);

% interpolating velocity values between two different positions (radius)
r5=(r1+r3)/2;
r_case5=linspace(r5,r5,300); % radius at laser position 5

for i=1:300
    u_i_case5(i,1)=((r3-r5)/(r3-r1))*M(i,2)+((r5-r1)/(r3-
r1))*M(i,4);%interpolation
end


r6=(r4+r1)/2;

r_case6=linspace(r6,r6,300); % radius at laser position 6
for i=1:300
    u_i_case6(i,1)=((r4-r6)/(r4-r1))*M(i,2)+((r6-r1)/(r4-r1))*M(i,5);
%Interpolation
end
```

```
%saving the interpolated values in the matrix M
M(:,6)=u_i_case5;
M(:,7)=u_i_case6;
M(1,:)=0;

% required steps in order to get the surface plot
% a new matrix, Z, is created here. The velocity values are rearranged in
% crescent order according to the value of the radius; so the column 1 are
% the velocity values corresponding to the lowest radius and the last
column is the values corresponding to the largest radius

r=[r1,r2,r3,r4,r5,r6];
rr=flip(r);
rrr=sort(rr)';

for i=1:1:n
Z(i,1)=M(i,4);
Z(i,2)=M(i,6);
Z(i,3)=M(i,2);
Z(i,4)=M(i,7);
Z(i,5)=M(i,5);
Z(i,6)=M(i,3);

end

[X,Y]=meshgrid(rrr,d(1:n)); %mesh for the surface plot
surf(X,Y,Z) %surf function
xlabel({'Radius';'  [mm]'});
ylabel({'Distance from Bottom to Top','          [mm]'});
zlabel({'u Component';'[mm/s]'});
title({'Fluid Flow Velocity Profile';'in the Stream Direction 80 RPM'});
grid
colorbar
%dlmwrite('matrix d and u.txt',M)
%dlmwrite('radius vector.txt',r)
xlabel({'Radius';'  [mm]'});
ylabel({'Distance from Bottom to Top','          [mm]'});
zlabel({'u Component';'[mm/s]'});
title({'Fluid Flow Velocity Profile';'in the Stream Direction 80 RPM'});
grid
colorbar

%steps for plotting the 3D liquid velocity profile
figure
plot3(r_case1,M(:,1),M(:,2));
set(gca,'Xdir','reverse');
xlabel({'Radius';'  [mm]'});
ylabel({'Distance from Bottom to Top','          [mm]'});
zlabel({'u Component';'[mm/s]'});
title({'Fluid Flow Velocity Profile';'in the Stream Direction 80 RPM'});
%axis ij
hold on
plot3(r_case2,M(:,1),M(:,3));
plot3(r_case3,M(:,1),M(:,4));
plot3(r_case4,M(:,1),M(:,5));
plot3(r_case5,M(:,1),u_i_case5,'--');
plot3(r_case6,M(:,1),u_i_case6,'--');
hold off
legend ('case1','Case2','Case3','Case4','Case5','Case6');
grid
```

```
%steps for plotting 2D liquid velocity profile
figure
plot(u_case3,d_case3);
hold on
plot(u_case1,d_case1)
plot (u_case4,d_case4)
plot (u_case2,d_case2)

xlabel('Fluid Velocity [mm/s]');
ylabel('Distance from bottom to top [mm]');
title('Fluid velocity profile for 80 RPM');
legend('case3 r=100.1 mm','case1 r=120.2 mm','case4 r=134 mm','case2
r=136.8 mm')
```

Appendix C

C. Illustrations

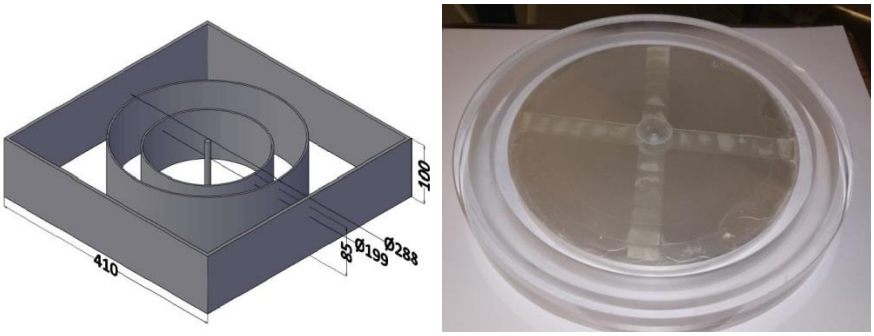

Figure C - 1: 3D setup and upper plate or lid. Note that the lid is not transparent

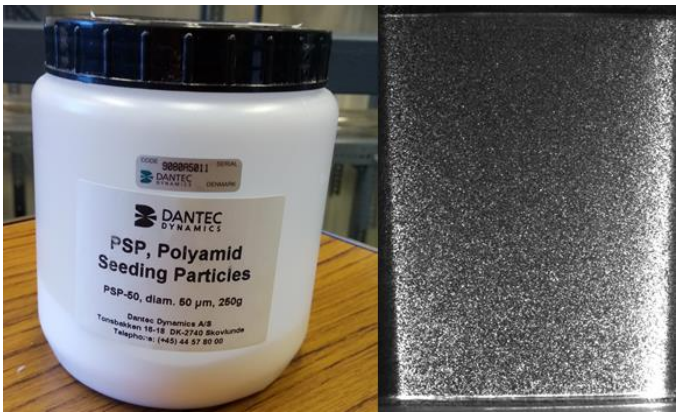

Figure C - 2: Seeding particles

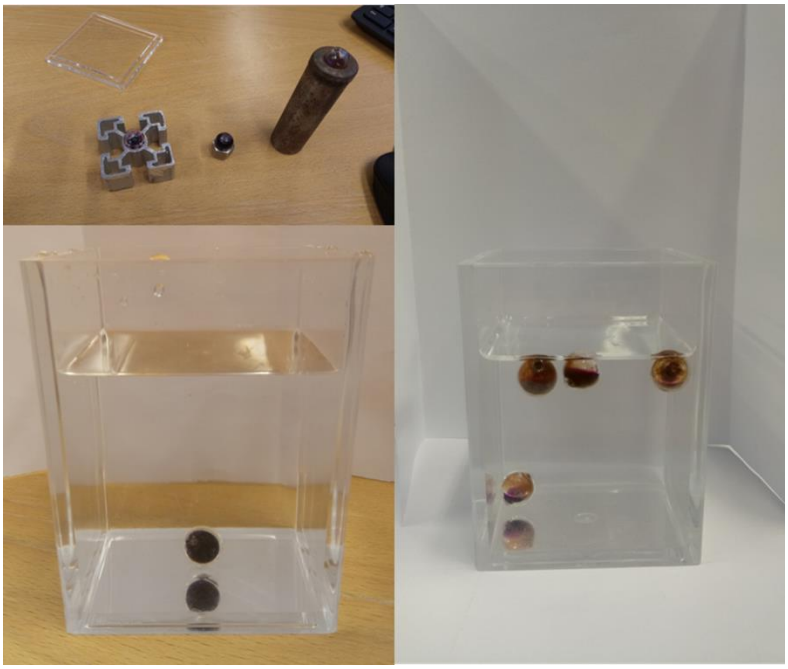

Figure C - 3: Design and test of the “Neutral glass particles”

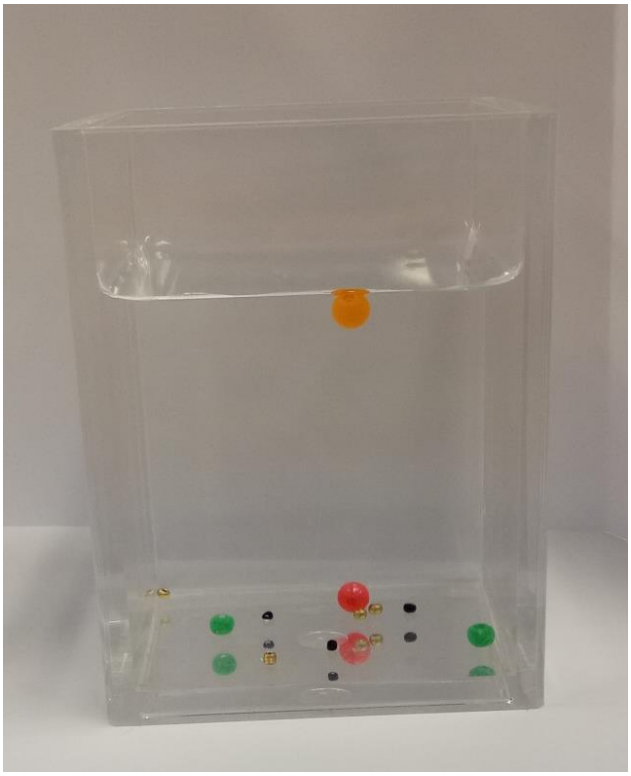

Figure C - 4. Test of " neutral plastic particles"

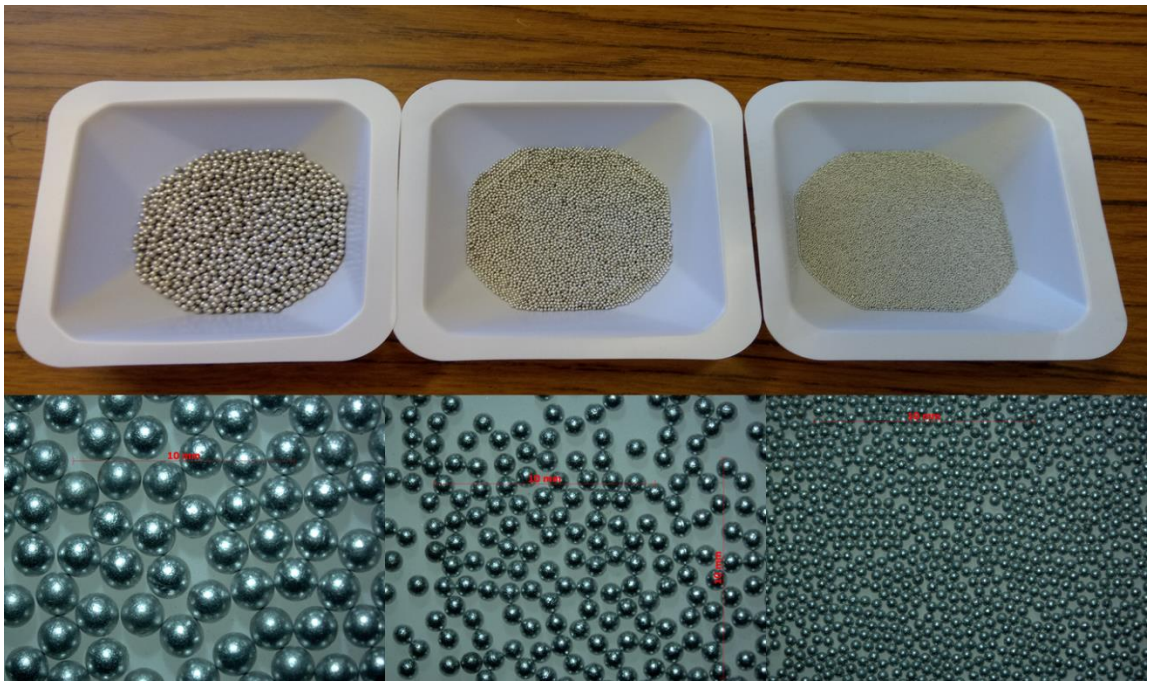

Figure C - 5: Aluminum spherical particles. Front left to right: 2 mm, 1 mm and 0.5 mm mean diameter.

Figure C - 6: Weighing scales –weight of the particles

Figure C - 7: Tools and equipment to make flat particles

Figure C - 8: Homemade Aluminum flat particles